

## Summary

Comments of referee #1. ....	1
Comments of referee #2. ....	18
Comments of referee #3. ....	33
List of relevant changes made in the manuscript .....	50

## Comments of referee #1.

The introduction states that the overall purpose of this study is to improve the surface rain rate retrieval calculated with the BRAIN algorithm from satellite measurements. How this shall be accomplished is not mentioned anywhere in the manuscript.

*We propose to rewrite parts of the introduction in order to clarify more context and purpose of this study:*

*“The French-Indian satellite Megha-Tropiques, launched in 2011, is primarily devoted to improve our knowledge about the life cycle of tropical convective systems over ocean and continents, the environmental conditions for their formation and evolution, their water budget, and the associated water vapor transport. For cloud studies, the most relevant instrument on the Megha-Tropiques satellite is the MADRAS microwave imager with 9 frequencies (18.7 GHz to 157 GHz). Similar satellite missions for tropical cloud studies are TRMM (Tropical Rainfall Measurement Mission, Huffman et al. 2007; Jensen and Del Genio 2003) or SSM/I (Special Sensor Microwave/Imager, Spencer et al. 1989). In order to retrieve the surface rain rate from brightness temperatures measured in the frame of above satellite missions, retrieval algorithms, as for example BRAIN (Viltard et al. 2006), are utilized. These retrieval algorithms have major sources of uncertainty due to the variability of the density of ice crystals in the tropical atmosphere.*

*With intent to learn more about the variability of crystal density in tropical convective clouds, two aircraft campaigns (presented in more detail in section 2) were associated to the Megha-Tropiques project. The campaigns have been conducted in order to get a better statistical description of the microphysical properties of hydrometeors in Mesoscale Convective Systems (MCS) in tropical regions. “*

Since, as this work shows, the retrieved coefficients are highly variable and also differ between the different clouds (here maritime and continental) one cannot readily use the coefficients found in this study for deriving cloud water content (CWC) from other measurements.

*This study suggests to determine the variability of the  $\beta$  exponent of the mass-diameter ( $m$ - $D$  :  $m=\alpha D^\beta$ ) relationship through the variability of the exponent  $\sigma$  of the surface-diameter ( $S$ - $D$ :  $S=\gamma D^\sigma$ ) relationship along the flight track. The  $S$ - $D$  relation is a power law which can be directly calculated from the images of optical array probes (here 2DS and PIP) for other relevant data sets. In this study,  $S$ - $D$  is calculated with a temporal resolution of 5 seconds by fitting the surface of the hydrometeors as a function of their  $D_{max}$  with a power law. Then, either the user has a bulk measurement of IWC to constrain  $\alpha$ , or may use the  $\alpha$  parameterizations as a function of  $\beta$ , and  $T$ , as presented in this study.*

ice/water:

For your calculations you assume that all cloud particles are ice. Did you confirm this? Or can you prove that it is a valid assumption, since measurements were clearly taken at temperatures where clouds could be mixed-phase. Assuming ice when it is water would result in an error in the calculation of the CWC due to the different density.

*In order to identify cases where the mixed phase (ice and water) was present, signals of the Rosemount Ice Detector have been analyzed. The RICE probe is in fact a supercooled water detector. We identified only very few and extremely short cases where the RICE probe showed supercooled water, when occasionally crossing young but small updraft cores. These rare data of supercooled water can be easily excluded from  $m(D)$  calculations for ice.*

Measurement uncertainties:

The instrumentation is described briefly, which is generally ok. However, what is missing is the important description of measurement errors and uncertainties. Every single one of them will propagate into the retrieval of the coefficients of the  $m(D)$  power law relationship and thus into the retrieved CWC. Therefore, a detailed discussion about measurement uncertainties and how they affect the retrieval is inevitable.

In detail:

What are the error margins of RASTA? It has huge error bars in Figure 11. What errors occur in the measurements of the cloud particle instruments, e.g. regarding number concentrations and sizes?

*RASTA calibration error and measurement error are in general taken together and estimated to 2dBZ. In figure 11, error bars do not represent the uncertainty on the measurements of RASTA, but the standard deviation with respect to the average of all the reflectivities measured in a layer of 5 Kelvin.*

*The uncertainty in the concentration of hydrometeors is estimated by the probe suppliers to be 20 %. This uncertainty stems mainly from the calculations of the sampling volume (DOF as fct of particle size, TAS), which is a function of particle size. An uncertainty of 20 % on the measured concentration gives approximately an uncertainty on  $\alpha$  of about 20 %.*

*Explanation:*

*As CWC is “independent” of the particle concentrations (let’s assume an error of 20%):*

$$CWC = \int_0^{\infty} N_1(D) \cdot \alpha_1 \cdot D^\beta \cdot dD = \int_0^{\infty} N_2(D) \cdot \alpha_2 \cdot D^\beta \cdot dD$$

then the uncertainty on the concentrations is not a function of diameters. Also the exponent  $\beta$  is not impacting because the uncertainty is available equally for all diameters. Then

$$\text{if } N_1(D) = (1 \pm \frac{\Delta N}{N}) \cdot N_2(D)$$

$$\text{then } \alpha_1 = (1 \mp \frac{\Delta N}{N}) \cdot \alpha_2$$

Therefore, an uncertainty of 20 % on the measured concentration gives an estimated uncertainty for  $\alpha$  of roughly 20 %.

Under the conditions where the measurements were taken, a high amount of shattering can be expected. A more detailed discussion in this regard would be highly desirable. How much data had to be removed due to shattering (is there a correction for the loss of data?), and thus, how does that propagate into the CWC retrieval? Can you demonstrate that the methods you use to identify and remove shattering do suffice? And please also give a short description of these methods, do not only cite the corresponding articles (so the reader has to look into those articles to find out what the correction does).

*First of all we have to point out that we always try to use most efficient newest probe tips to avoid shattering. This is valid for 2D-S and PIP probes used during the two Megha-Tropiques measurement campaigns. Only after minimizing shattering, we subsequently apply software to cleanse the data from shattered particles, etc. Distinction between natural particles and the particles resulting from the shattering is performed by analyzing the inter-arrival time between two neighboring particles. Occurrences of inter-arrival times are modeled with the help of Poisson distributions. When shattering is present, the probability of the inter-arrival time of shattered particles and the probability of inter-arrival time of the natural particles are modeled by two different Poisson distributions. The analysis is performed continuously with packages of 20000 particles, which allows taking into account the inhomogeneity of clouds along the flight track, especially with significant variations in particle number concentrations. Hence, we can deduce a threshold time which allow to separates the two populations of particles. However, also some of the natural particles can be eliminated, if the two modes are too close to each other. The size distribution is corrected for this. Our method is widely used, and many discussions can be found in further publications. We have decided not to detail the shattering subject here. The details of the algorithm have been presented at the 2012 ICCP conference:*

(R. Dupuy, C. Duroure, A. Arthur, and A. Schwarzenboeck. Particle inter-arrival time analysis and shattering removal at high sampling speed and high particle concentration in mesoscale convective system. ICCP International Conference, Leipzig 2012.)

*For example figure 1a, illustrates the differences between two PSD (without and with removal of shattered particles  $PSD_{diff} = PSD_{with\ shattering} - PSD_{no\ shattering}$ ).*

*Figure 1b)-c) et d), shows three individual PSD of 5-second time intervals.*

Without applying the anti-shattering algorithm (and compared to the data when the anti-shattering algorithm is applied), surface-diameter relationships are little impacted on average and the exponent  $\beta$  of  $m$ - $D$  increases slightly by approximately +4%. The retrieved prefactor  $\alpha$  from the measured and simulated reflectivities and PSD is impacted by about +25%, and CWC increases by about +5%.

The error estimation has been performed according to:

$$\frac{100 * \Delta X}{X} = 100 \frac{(X_{withshattering} - X_{withoutshattering})}{X_{withoutshattering}}$$

where  $X$  can be  $\alpha_\sigma$ ,  $\beta_\sigma$  and  $CWC(\alpha_\sigma, \beta_\sigma)$

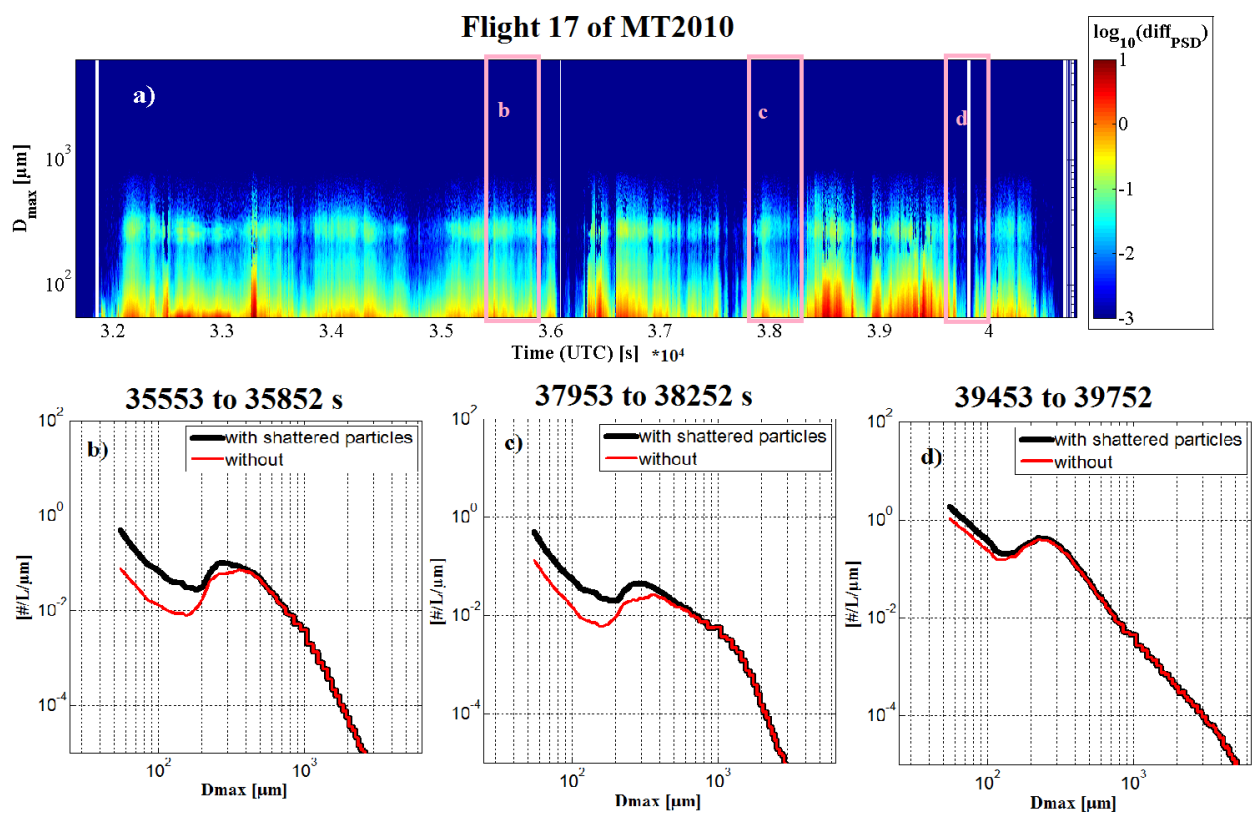


Figure 1 a) Contour plot of the logarithm of PSD containing shattered particles minus the respective PSD where shattered particles have been removed, as a function of the  $D_{max}$  on the y-axis and time (seconds after midnight) on the x-axis. 1b-d) in black the PSD containing still the shattered particles, in red PSD after shattering removal.

Full use of dataset:

Furthermore, how do you derive  $\gamma$ (equation10)? Don't you also need  $\gamma$  to derive  $\sigma$ ?

$S$ - $D$  are calculated for 5-seconds steps and are synchronized with PSD and RASTA reflectivity. To calculate  $S$ - $D$ , we plot the mean surface of the particles versus their  $D_{max}$  (figure2) for the two probes.  $S$ - $D$  relation then is fitted by a power law described by two parameters: prefactor  $\gamma$  and exponent  $\sigma$ , for both probes, respectively. On a log-log scale,

$\ln(\gamma)$  represents the y-axis intercept and  $\sigma$  the slope of the linear relationship such that  $\log(S) = \sigma \cdot \ln(D) + \ln(\gamma)$ .

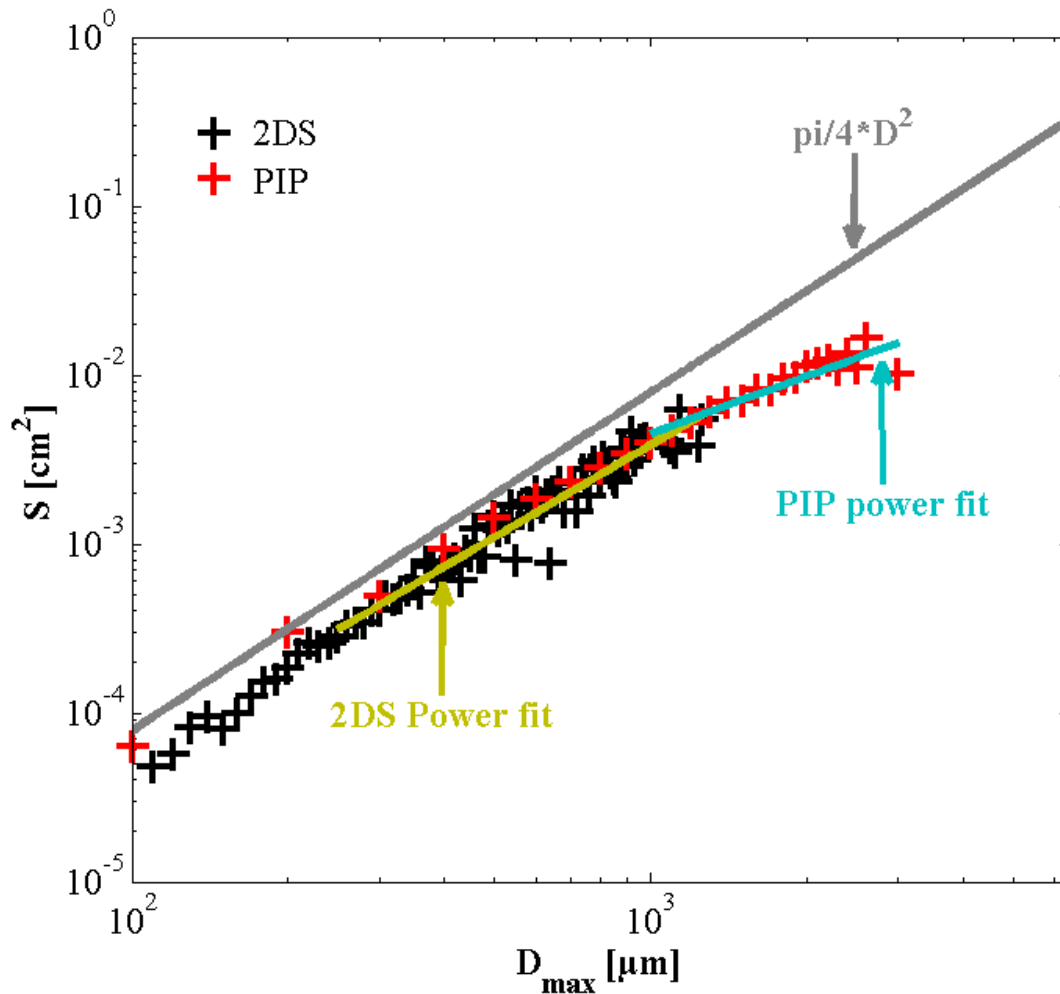


Figure 2 : Mean projected surface in  $\text{cm}^2$  on y-axis versus  $D_{\text{max}}$  in  $\mu\text{m}$  on the x-axis. Black symbols represent the 2DS image data and red symbols the PIP data. The grey line would be the power law fit for spherical particles. The golden line is the power law which fits the 2DS data for  $D_{\text{max}}$  larger than  $250\mu\text{m}$  and the blue line fits the PIP data with a power law for  $D_{\text{max}}$  larger than  $950\mu\text{m}$ .

In the first instance you use 2DS and PIP measurements to derive  $\alpha$  and  $\beta$ . However, from Section 4 on, you only use the 2DS measurements for calculating the surface diameter relationship and use this to derive  $\beta$ . You correctly say that it is better to use 2DS images for sub-millimetric particles, but for the larger crystals you will still gain shape information from the PIP images as well. So, why not using 2DS images for the smaller particles and PIP images for the larger particles?

*S-D relationships calculated for sub millimetric (2DS) and millimetric particles (PIP) can deviate. Retrieving m-D relationships for two probe specific (2D-S and PIP) power laws would imply that we need to solve one equation with two unknowns:  $\alpha_{2DS}$  and  $\alpha_{PIP}$  (eventually three, since we need to know the application range of both m-D relationships in terms of a diameter  $D_c$  separating both laws).*

$$CWC = \sum_{D_{\max}=55\mu m}^{D_{\max}=Dc} N(D_{\max}) \cdot \alpha_{2DS} \cdot D_{\max}^{\beta_{2DS}} \cdot \Delta D_{\max} + \sum_{D_{\max}=Dc}^{D_{\max}=6450} N(D_{\max}) \cdot \alpha_{PIP} \cdot D_{\max}^{\beta_{PIP}} \cdot \Delta D_{\max}$$

In the following step for retrieving  $\alpha$ , you use again the combined measurements. Wouldn't this be a source of error?

*The use of the S-D relationship allows representing the variability of the exponent  $\beta$  of the m-D relationship as a function of the actual 2D images which are recorded. And even if  $\beta$  would be determined from 2D-S images only and thus the exponent  $\beta$  is not carrying most correctly the information of super-millimetric crystals from PIP images, the prefactor  $\alpha$  will always somewhat compensate for that. Once the exponent  $\beta$  is estimated from  $\sigma$  as a function of time, the prefactor  $\alpha$  is calculated in order that the simulated reflectivity is equal to the measured reflectivity. The prefactor  $\alpha$  is constrained such that all the hydrometeors follow the same m-D.*

What would the difference be between  $\beta_{\sigma}$  when only using 2DS images and  $\beta_{\sigma}$  when using images from both instruments?

*Calculating a single S-D power law relationship by fitting simultaneously the data points of the 2DS ( $250\mu m < D_{\max} < 1mm$ ) and the data points of the PIP ( $D_{\max} > 1mm$ ) may not produce an ideal and thus realistic S-D power law for the combination of both probes.*

*Therefore we will introduce for the revised version of the manuscript a  $\sigma$  exponent taking into account simultaneously 2DS and PIP images. This particular  $\sigma$  is calculated by weighting  $\sigma$  of each probe with the ratio of the surface of ice crystals contained in the size range of the individual probe (size range where individual S-D relationship is calculated) over the entire surface within the total size range covered by both probes:*

$$\sigma = \frac{\sum_{D_{\max}=250\mu m}^{950\mu m} N(D_{\max}) \cdot S(D_{\max})}{\sum_{D_{\max}=250\mu m}^{6450\mu m} N(D_{\max}) \cdot S(D_{\max})} \cdot \sigma_{2DS} + \frac{\sum_{D_{\max}=950\mu m}^{6450\mu m} N(D_{\max}) \cdot S(D_{\max})}{\sum_{D_{\max}=250\mu m}^{6450\mu m} N(D_{\max}) \cdot S(D_{\max})} \cdot \sigma_{PIP}$$

*Figures 3 and 4 show the differences of relationships between  $\alpha_{\sigma}$  and  $\beta_{\sigma}$ , when  $\sigma$  is calculated from 2DS and PIP images (figure 3), and when  $\sigma$  is only calculated from images of the 2DS (figure 4).*

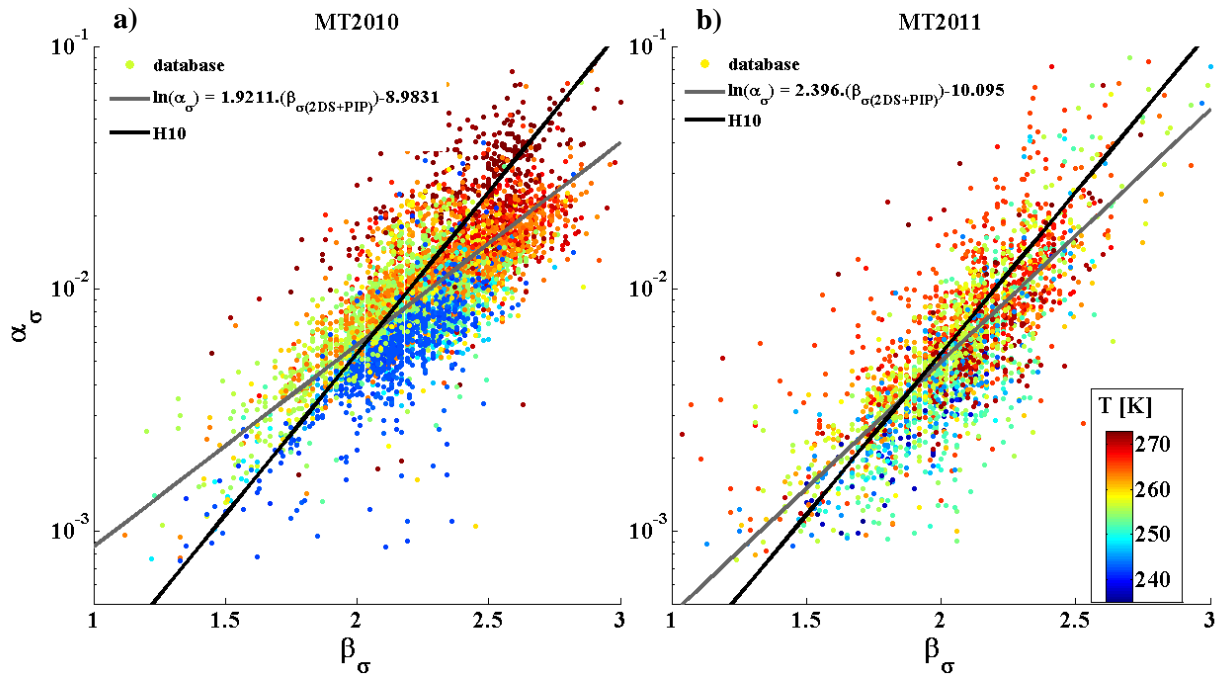


Figure 3 : a)  $\beta_\sigma$  versus  $\alpha_\sigma$  for MT2010, where  $\beta_\sigma$  has been derived from  $\sigma$  which is calculated from 2D-S plus PIP images. b) same as a) but for MT2011.

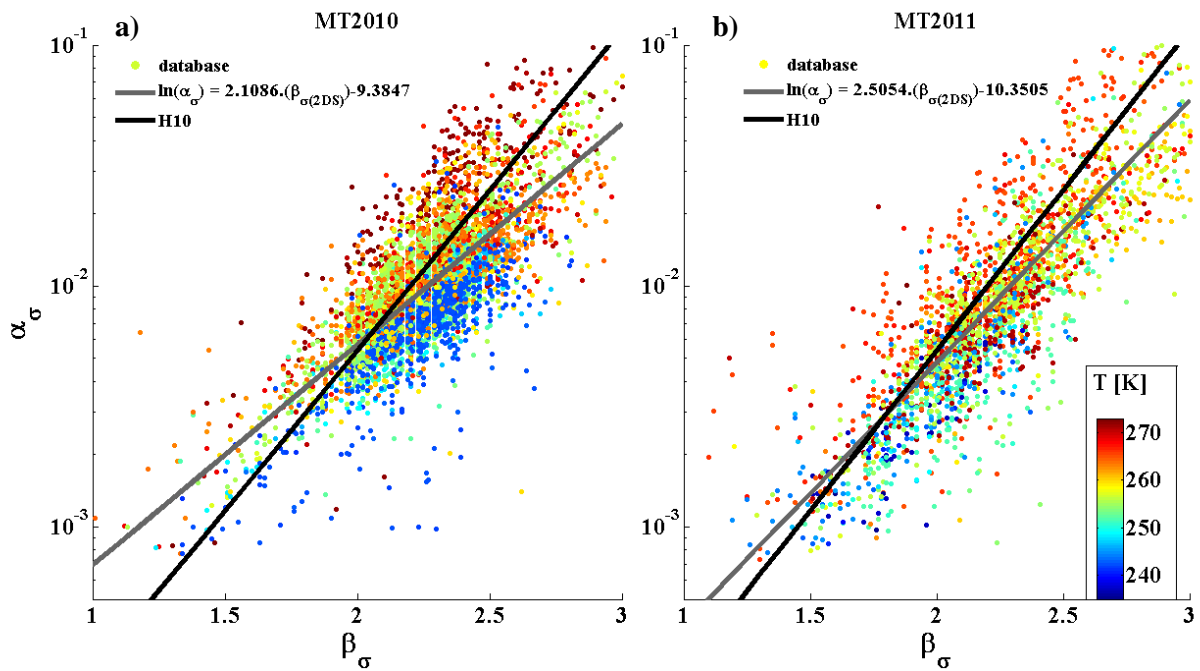


Figure 4 : Same as figure 3, but  $\beta_\sigma$  derived from  $\sigma$  which is solely calculated from 2DS images.

### Specific comments

Page 2984 line 20: “concentrations of the hydrometeors increase with altitude” Please mention to what altitude layer you are referring, other studies have shown the opposite behaviour when looking at higher altitudes. Thus, it is an important additional information.

*Also with respect to the comments of the second reviewer we now state in the revised manuscript :*

*“between the 270K level and the 230K level, the mean profile of the concentration of hydrometeors shows an increase of concentrations with altitude.”*

Page 2988 line 15-22: Please indicate the size range covered by the instruments.

*“Next to the Doppler Cloud radar RASTA (Protat et al. 2009) in-situ measurements of microphysical properties were performed using a new generation of Optical Array Probes (OAP): the 2-D stereo probe (2DS) from Stratton Park Engineering Company (SPEC) Inc. which allows to monitor 2D images in the size range 10-1280 $\mu$ m, and the Precipitation Imaging Probe (PIP) from droplet Measurement Technologies (DMT) which measured hydrometeors in the size range from 100-6400  $\mu$ m.”*

Page 2990 line 7: Does it make sense to specify a bin width of 10 microns also in the size range where measurements are purely taken by the PIP? Have you considered an increasing bin width with increasing particle size?

*To handle a composite PSD from the two probes, we needed to put them to the same resolution. In order to not lose information given by the 2DS for small sizes of hydrometeors we wanted to keep its resolution (10 $\mu$ m). Artificially increasing the PIP resolution to 10 $\mu$ m pixel just keeps all the original information of the 100 $\mu$ m pixel resolution. No interpolation, just keeping all the information of the original data.*

*And: No, we did not consider an increasing bin width with increasing particle size.*

Page 2992 line 13/14: 2gm<sup>-3</sup> of spread in CWC sounds very much. How much is it percentage-wise?

*Indeed 2gm<sup>-3</sup> of spread in CWC is quite high. But on average the spread is evaluated to be 25% of the retrieved CWC.*

Page 2993 line 8-10: What is a typical measurement error for RASTA (besides the mentioned calibration error)?

*Calibration error and measurement error are in general taken together and estimated to 2dBZ.*

How high are uncertainties in the CWC retrieval if RASTA uncertainties are taken into account?

*Related uncertainties are given in table 2. In case that the error due to the calibration is around 2dBZ, this impacts the CWC retrieval by +/- 25%.*

Page 2999 line 2/3: While you only use two flights for the analysis for MT2011, I wonder why you don't also use the other two flights stated in Table 1 as a third class – oceanic isolated convective system?

*For the isolated oceanic convective systems, relatively few data are available. So for statistical purposes, we consider the dataset of isolated oceanic convective systems not sufficient.*

Page 2999 line 14: I am sceptical if you can see a decrease of  $\beta_\sigma$  with altitude. I would say it is fairly constant, also taking the error bars into account.

*“Figure 11b illustrates the trends of  $\beta_\sigma$ , its mean profile shows a small decrease with altitude for MT2010, but it seems not significant accounting the variability of  $\beta_\sigma$  at a given altitude.”*

Page 2999 line 19: Houze 2004 would be a good reference here.

*“MCS systems are composed by a convective part in the front of the systems and a trailing stratiform part (Houze 2004).”*

Page 2999 line 24: Are the clouds in SH2010 continental or maritime?

*“In addition, our results are compared with two types of vertical profiles given in SH2010. The first profile was obtained from the dataset of the CRYSTAL-FACE project (clouds were formed from land and sea breeze convection in the southern part of Florida; represented by the blue line in figure 11) and the second profile stems from a dataset of ARM (clouds were synoptically generated above the North American continent, Oklahoma ; represented by the dashed blue line in figure 11).*

$$m = (0.0102 + 0.00013 \cdot (T - 273.5)) \cdot D^{(2.4+0.0085(T-273.15))} \quad [\text{CRYSTAL - FACE}] \quad (X)$$
$$m = (0.0064 + 0.000095 \cdot (T - 273.15)) \cdot D^{(2.1+0.0036(T-273.15))} \quad [\text{ARM}]$$

“

Page 3000 line 2: You refer to Figure 12d, I assume you mean Figure 11d?

*The reviewer is right, however, these parts of the text which describe figure 11 c, d, and f have been deleted, to take into account the comments of the 2<sup>nd</sup> referee.*

Page 3000 line 7-14: I cannot see a general decrease of CWC with altitude for the MT2010 case. I can rather see an increase in the lower levels and than a more or less constant behaviour. A decrease is only visible if you look solely at the uppermost three points.

*This part of the text and corresponding figure 12 has been deleted to also take into account the comments of the 2<sup>nd</sup> referee.*

Page 3001 l 5/6: “..., while this decrease is less pronounced for MT2011” - I can hardly see a decrease!

*This part of the text and corresponding figure 12 has been deleted to also take into account the comments of the 2<sup>nd</sup> referee.*

Page 3001 line 7/8: “This observational result may be due to low number of samples available in the high altitude during MT2011.” From Figure 11 I still read about 30 samples here (at minimum at 240K). I recommend deleting this sentence.

*This part of the text and corresponding figure 12 has been deleted to also take into account the comments of the 2<sup>nd</sup> referee.*

Page 3001 line 22-24: For the decrease in the uppermost part (<245K), are you comparing more than two temperature bins? I would leave this sentence out.

*This part of the text and corresponding figure 12 has been deleted to also take into account the comments of the 2<sup>nd</sup> referee.*

Page 3002 line 4-6 (and following part): As you mention, a good correlation between CWC and radar reflectivity is no surprise since you use the reflectivity to derive CWC. So, of what use is this correlation then? Why are you doing it?

*Literature provides a lot of Z-CWC relationship at 94GHz (and 35GHZ) where in general CWC has not been constrained by the reflectivity or using only Mie calculations. Hence it is interesting to confront our relationships with other relationships presented in literature for tropical regions.*

Page 3004 line 27: As mentioned above, I am not convinced that  $\beta$  decreases in the MT2011 case.

*“ It is clearly found that the variability of the  $m(D)$  coefficients  $\alpha_\sigma$  and  $\beta_\sigma$  is large. Mean profiles of this coefficient can be fitted as a function of the temperature (equation X for 2DS+PIP and equation X+1 for only 2DS) and gives smaller values for cold temperatures than for temperatures near the melting layer.*

$$\begin{aligned} \text{MT2010:} & \begin{cases} \ln(\alpha) = -0.37459 \cdot T - 14.1809 \\ \beta = 0.008928 \cdot T - 0.041 \end{cases} \\ \text{MT2011:} & \begin{cases} \ln(\alpha) = -0.003306 \cdot T + 0.7431 \\ \beta = 0.0064105 \cdot T + 0.41 \end{cases} \end{aligned} \quad (X)$$

$$\begin{aligned} \text{MT2010:} & \begin{cases} \ln(\alpha) = 0.02999 \cdot T - 12.164 \\ \beta = 0.0025413 \cdot T + 1.61 \end{cases} \\ \text{MT2011:} & \begin{cases} \ln(\alpha) = -0.00018 \cdot T^3 + 0.1341 \cdot T^2 - 33.132 \cdot T + 2715.9 \\ \beta = 5.10^{-5} \cdot T^3 + 0.0037986 \cdot T^2 - 9.4078 \cdot T + 776.66 \end{cases} \end{aligned} \quad (X+1)$$

“

Page 3005: In the discussion about differences between continental and oceanic convective systems, I would appreciate some references to previous studies that show differences in those clouds. E.g. Cetrone and Houze, 2009, Frey et al., 2011.

*“Continental MCS in the monsoon seasons are due to the convergence of wet colder air masses from the ocean with dry warmer air masses, while over the Indian Ocean convection is due to the buoyancy of wet air masses leading to weaker convection in our case. Further studies (Cetrone and Houze 2009 ; Frey et al 2011) have discussed differences in the intensity of tropical convection between pure African continental MCS and more maritime MCS with*

*some continental influence (South Asia to the north of Australia). These studies conclude on deeper convective systems and strongest precipitation for African MCS.”*

Page 3006 line 2/3: I think that there are also aggregates visible in the images from MT2011.

*“For other levels ice crystal shapes are in general different. Besides aggregates, significant amounts of individual large pristine ice crystals such as dendrites (typically due to water vapor diffusion only) could be observed in MT2011.”*

Page 3007/3008: “...and in the fourth L is constant and equal to 16 pixels. L has been chosen out of the size range of [10;100] pixels with 1000 simulations for columns in each of the four cases.” I think one of the “L”s should be a “H”.

*“...and in the fourth L is constant and equal to 16 pixels. H has been chosen out of the size range of [10;100] pixels with 1000 simulations for columns in each of the four cases.”*

Figure 1:

The line from PIP measurements shows particles smaller 100 $\mu$ m, while that is the smallest size detectable for the PIP?!

*A pixel is shadowed, when more than 50% of the laser intensity is hidden, then a particle of more than 50 $\mu$ m can be represented by one pixel. It is the uncertainty on the size due to the PIP resolution.*

In Fig 1b, the PIP distribution starts at about 250 $\mu$ m, why is there such a difference in the PIP size range between the distributions in Fig.1a and Fig.1b?

*In fact, Fig1b also starts at 50 $\mu$ m, but the aspect ratio is equal to 1 between 50 and 150 $\mu$ m. The Aspect ratio of particles between 150 $\mu$ m and 250 $\mu$ m is not valid.*

How can the composite distribution differ from the 2DS distribution at sizes around 90 $\mu$ m?

*This is a mistake of different temporal integration, the time interval taken to plot this quicklook was not exactly the same for various PSDs. The composite PSDs have a time resolution of 5 seconds and the individual raw PSD of 2DS probes and PIP probes have a 1 seconds time resolution. Figures 1a and 1b include only one composite PSD (5seconds) and in addition the mean of 10 individual PSDs of 2DS and PIP probes. This has been corrected in the revised manuscript. New figures are presented below.*

While you mention a general good agreement between the two probes, I find the discrepancy in the overlap region at around 100 $\mu$ m and at around 1mm not negligible.  
Can you comment on these?

*The PIP PSD used to produce this figure has been also used to demonstrate the effect of the DOF flag attributed to individual particles (see user’s guide of CIP and PIP instruments from DMT Inc.). The DOF flag allows the user to know if the registered particles was considered*

as an out of focus particle or not. Of course we should not have used this one, but the one we use to produce the PSD composite.

In addition, the probability of truncated images of hydrometeors increases with its size. Therefore, for the 2DS as for the PIP, the larger diameter ends of the individual PSDs are noisy. Also the slopes are more important. Even if methods exist (and that we apply to correct for truncated particles), these methods are adapted for spherical particles rather than for complex shapes of ice crystals. The effect of the size reconstruction method (for truncated images) is more visible on the composite of the aspect ratio.

Below are the figure versions of all PSDs over the same 10 seconds of sampling time. In addition, the individual PSD presented for 2D-S and PIP probes are those that are used for the calculation of the composite PSD. We apologize for this mistake, but as this figure was considered just as a schematic quicklook of the method, our attention was not concentrated on that.

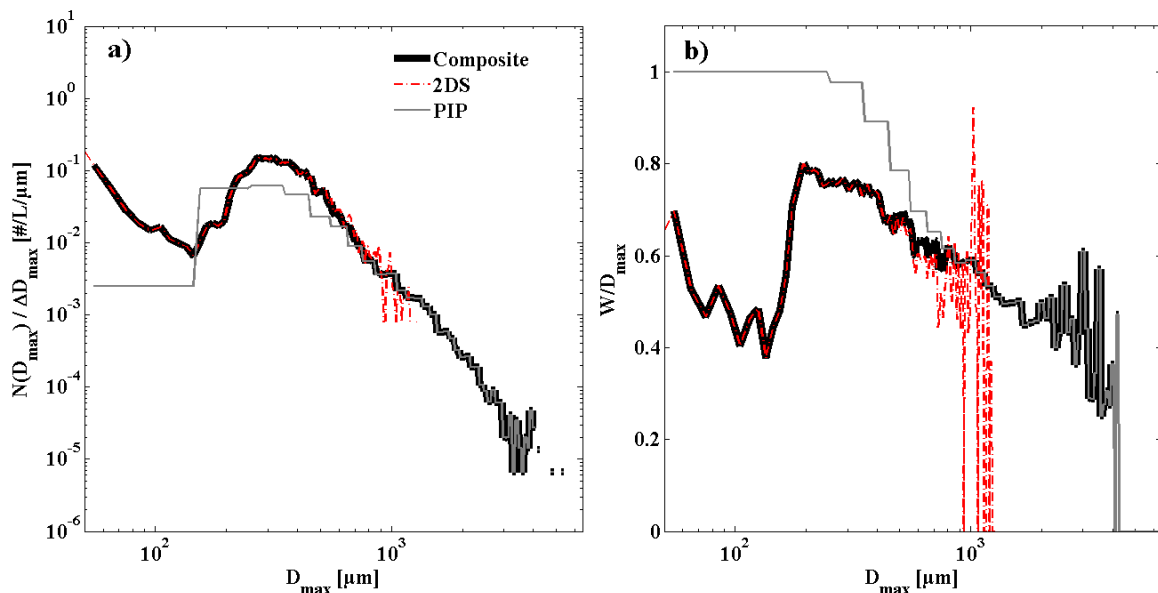


Figure 5 : a) Number size distributions (as a function of  $D_{max}$ ) of cloud particles. The dashed red line represents the 2D-S data, the grey line the PIP data, and the bold black line represents the composite particle number size distribution (PSD). b) Aspect ratio of 2D particles as a function of  $D_{max}$ . Symbols for 2D-S and PIP as above. All curves (number size distributions and aspect ratios) represent an average over 5 seconds of measurements.

Figure 2:

The caption says that you show the effective reflectivity  $Z_e$ , while the graph shows  $Q_{back}$ . What is correct?

“FIG. 2. Calculated backscattering cross section (in  $mm^2$ ) as a function of the maximum particle diameter  $D_{max}$  (in  $\mu m$ ). Pink, blue, green, red and cyan curves are calculated for different Aspect ratios by the T-matrix method, whereas the brown curve is based on the Mie theory calculation for a spherical particle. The black curve represents the Rayleigh approximation. “

Figure 6:

You may want to consider grouping these images according to their habit classes (and specify these on the plot).

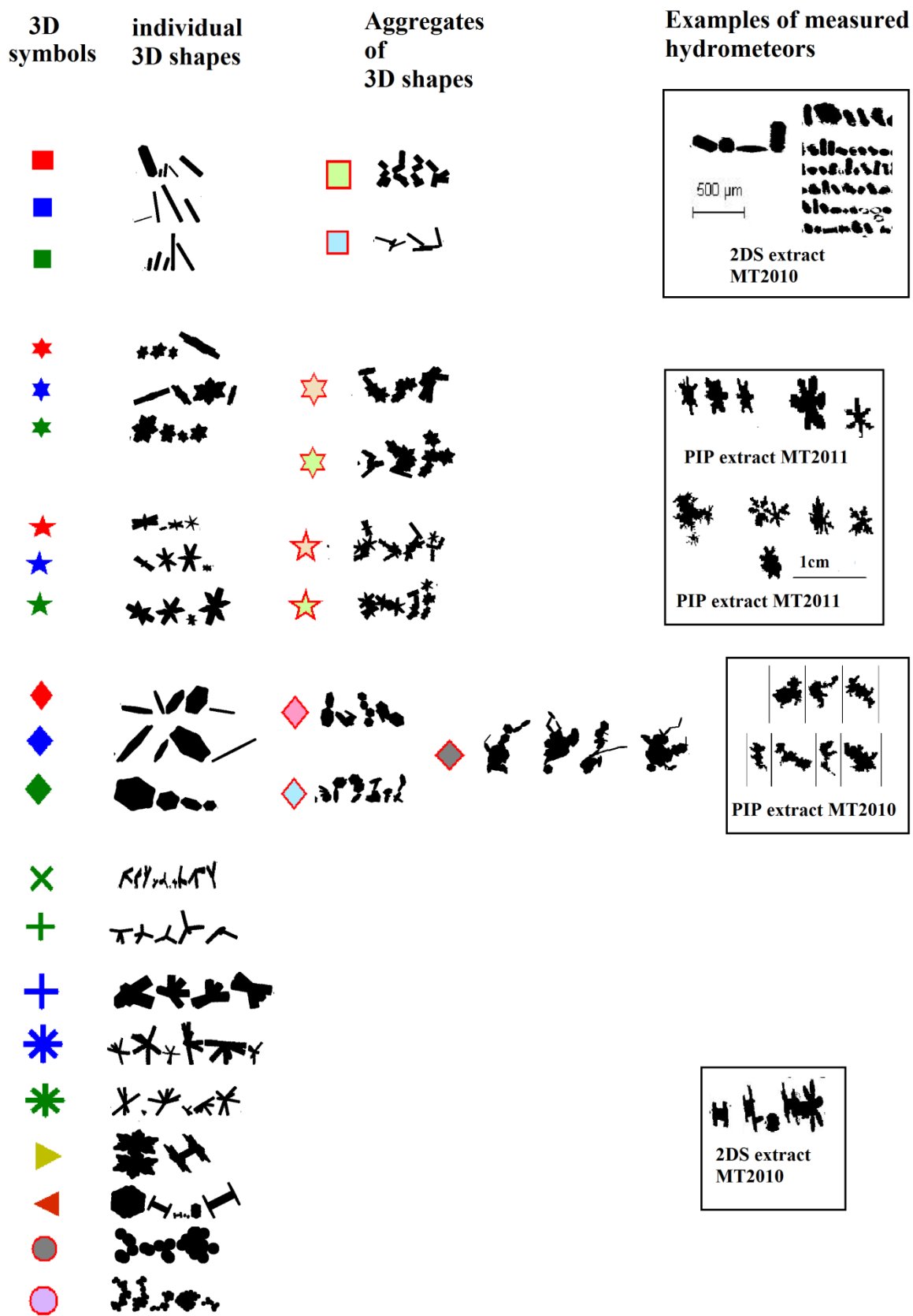


Figure 6 : On the left column are presented examples of 2D projections of randomly oriented 3D shapes of single hydrometeors with their corresponding symbols as they are represented in figure 7 and in table 4. In the middle column, examples of aggregates composed of single individual shapes as shown in the left column. The right column shows examples of crystals resembling what has been recorded in different aircraft measurement campaigns.

Figure 7:

The blue contours around the blue symbols are not recognisable. Changing the colours of the dark blue symbols would be desirable.

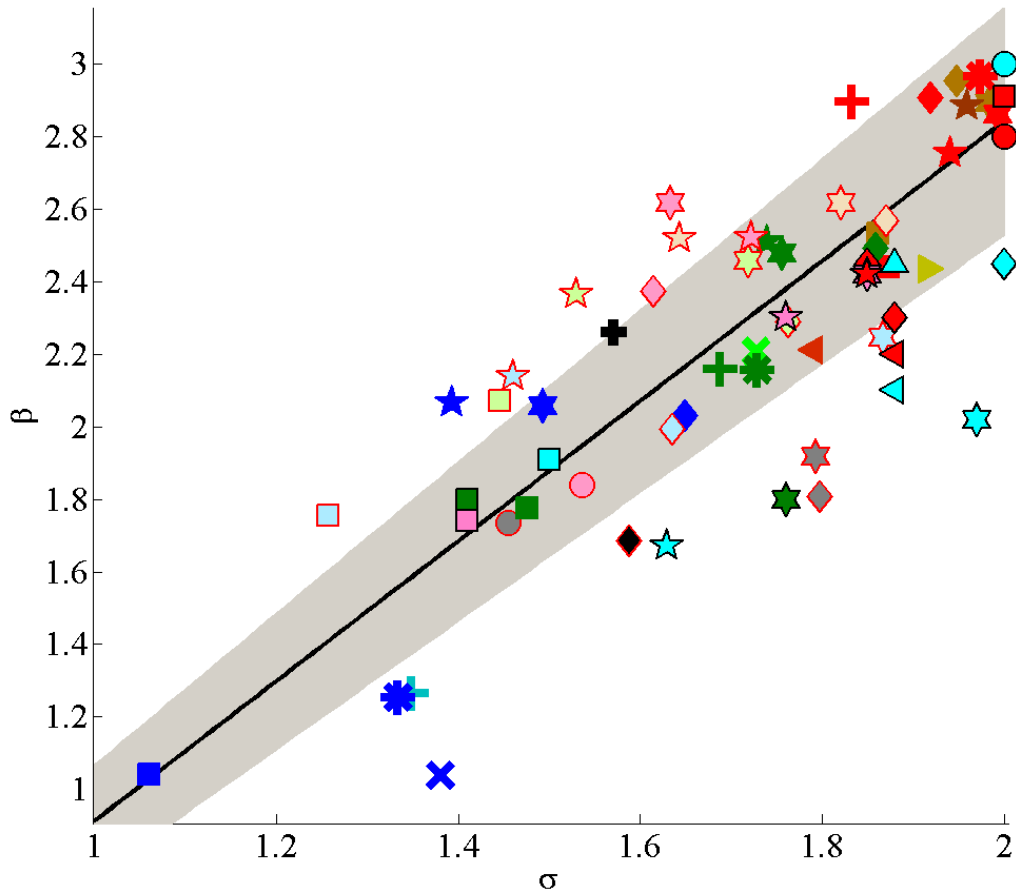


Figure 7 : Exponent  $\beta$  of  $m(D)$  relationships as a function of the exponent  $\sigma$  of the corresponding  $S(D)$  relationship. Each data point either with red contours or without contours is deduced for a population of 1000 simulated 3D shapes and corresponding projections. Symbols with red contours are deduced for 3D aggregates of crystals of an elementary shape. Symbols with black contours stem from Mitchell (1996). The legend for symbols is given in table 4. A linear fit of all simulated data is shown by the black line. The grey band represents the mean standard deviation (11%)

Figure 8:

Please add the subscript  $\sigma$  on  $\beta$  and  $\alpha$  (Fig 8c and d), the caption of Fig 8e says that CWC (black line) is deduced from  $\beta_\sigma$  and  $\alpha_\sigma$  while the annotation in the Figure suggests it's the average CWC deduced from  $\beta_i$  and  $\alpha_i$ . What is correct? Why are there gaps in the black line?

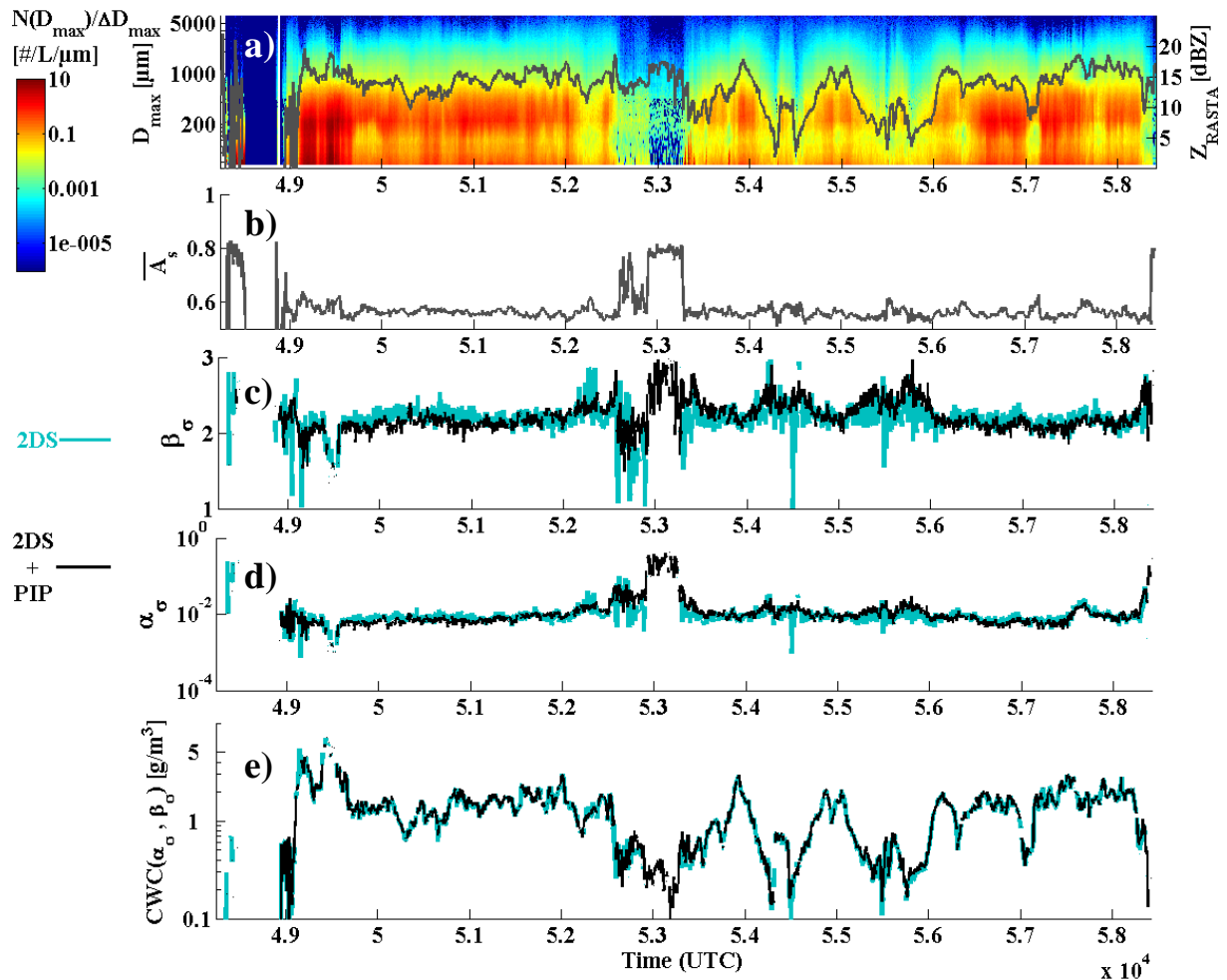


Figure 8 : (a) Contour plot of the time series of the number PSD (as a function of  $D_{\max}$ ) color coded with the number concentration in  $L^{-1} \mu m^{-1}$ , the grey line shows the simultaneously measured radar reflectivity (secondary y axis). (b) Mean aspect ratio along the flight. (c)  $\beta_{\sigma}$  exponent calculated from  $\sigma$  of 2DS in blue and from  $\sigma$  of 2DS plus PIP in black. (d) Pre-factor  $\alpha_{\sigma}$ , subsequently deduced from the T-Matrix method, for the corresponding  $\beta_{\sigma}$  above. (e) CWC calculated with  $\alpha_{\sigma}$  and  $\beta_{\sigma}$  presented above. In blue when  $m(D)$  is constrained by the submillimetric images of hydrometeors (2DS) and in black when  $m(D)$  is constrained by submillimetric (2DS) plus millimetric (PIP) images of hydrometeors.

Figure 11:

You mention in the text that data points around the melting layer have to be treated with care. Please indicate the melting layer on the plot (e.g. with a shading).

Figures 9 and 10 below are new figures to replace former figure 11. According to the 2<sup>nd</sup> referee we only keep vertical profiles of the  $m(D)$  coefficients. For clarity reasons, we added more details on the standard deviation and the mean profile. Data points are plotted in a kind of background. Figures 9 and 10 are shown, to continue to demonstrate what are the differences when estimating  $\beta_{\sigma}$  only from the 2DS probe images (figure 10) and from the images of the two probes (2DS plus PIP).

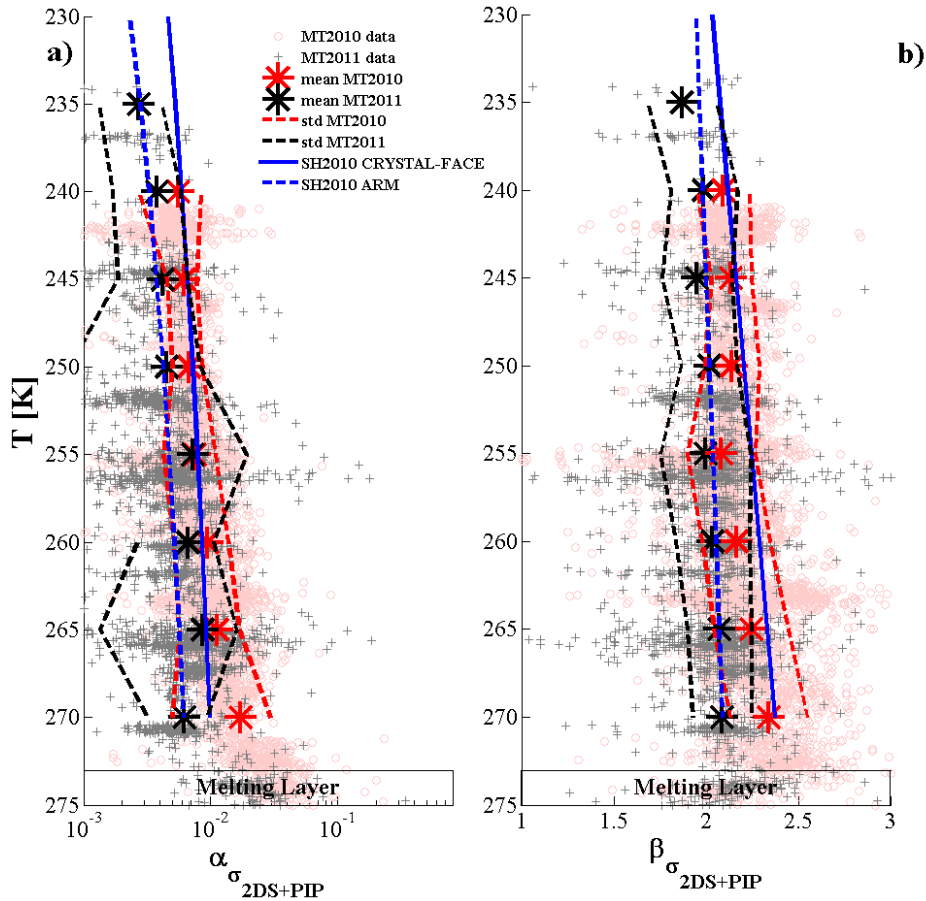


Figure 9 : Vertical profile of  $m(D)$  coefficients constrained by T-matrix and the variability of S-D exponent  $\alpha$  calculated from 2D-S plus PIP images. (a)  $\alpha_{\sigma}$  versus the temperature in K. (b)  $\beta_{\sigma}$  versus the temperature in K. Pink circle show data points (5-seconds time step) of MT2010, grey crosses show MT2011 data. Red and black stars present mean values of  $m(D)$  coefficients in 5K temperature intervals for MT2010 and MT2011, respectively. Dashed red and black lines show standard deviations of MT2010 and MT2011, respectively, from the mean value. Blue solid and dashed lines show vertical profiles of SH2010 obtained for CRYSTAL-FACE, and for ARM, respectively.

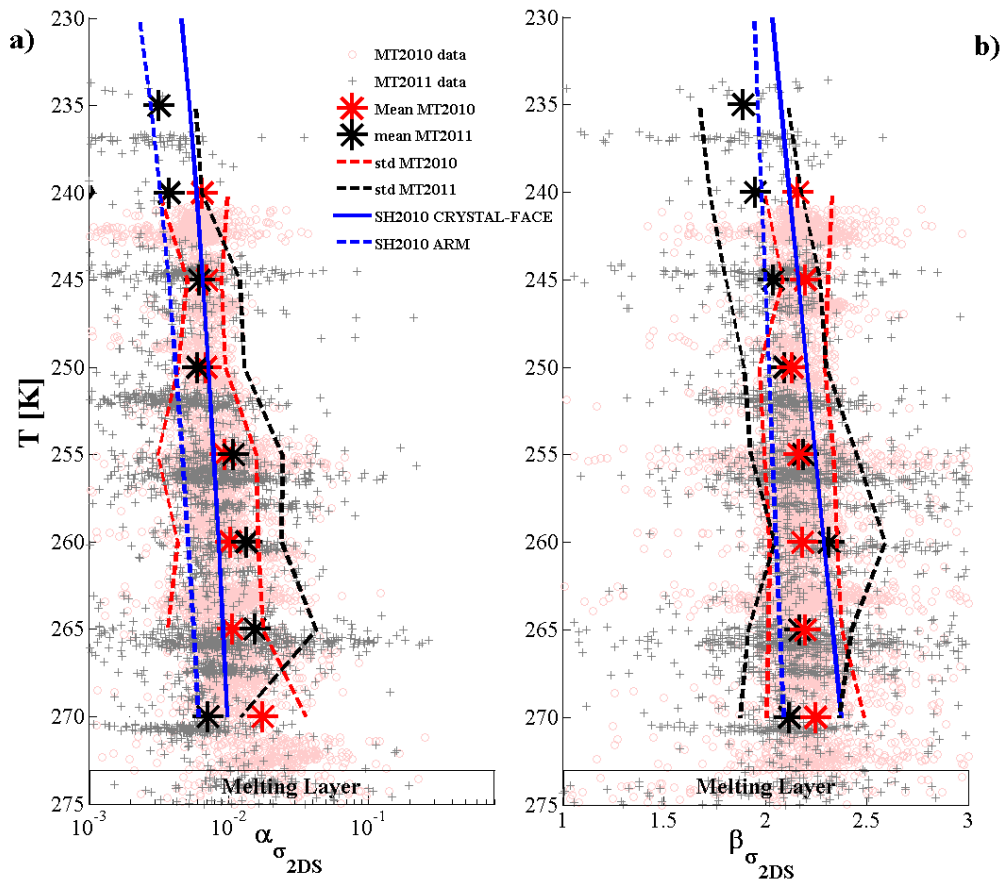


Figure 10 : Same as figure 9, but  $m(D)$  coefficients constrained by T-matrix and the variability of S-D exponent  $\alpha$  calculated from 2DS images only.

Why are there no error bars for the total number concentration? Please add.

*This part has been deleted according to the 2<sup>nd</sup> referee comment.*

Figure 12g-h:

You write equivalent reflectivity in the caption, in the Figure it says total backscatter coefficient ( $Q_{back}$ ), what is correct?

*This part has been deleted according to the 2<sup>nd</sup> referee comment.*

Figures 11 and 15:

The choice of colours in these figures is unfavourable for colour blind people. You may want to consider another colour pair.

*New version is shown above (new figures 9 and 10), and figure 15 has been deleted according to the 2<sup>nd</sup> referee comment.*

## Comments of referee #2.

Major comments (structure):

1. Introduction (p.2985, lines 14-22): This section requires more elaboration on the motivation of the study. What is the actual problem with fixed mass-diameter-relationship coefficients? Do we need them to vary with temperature? How will it help Megha-Tropiques retrievals or numerical simulations, especially when cloud-ice probe data and radar data are unavailable? Addressing the purpose more strongly in this section will give the paper clearer focus and should allow for better understanding of why certain figures and discussions appear later in the paper.

*The respective part in the introduction/motivation has been rewritten as follows:*

*“ The main focus of this study is to characterize the statistical relationship  $m(D)$  between mass and maximum diameter of ice crystals by developing a retrieval technique that combines radar reflectivity and particle imagery in order to produce reliable calculations of the condensed water content (CWC) as a function of time (along flight trajectory). More particularly, this study focuses on the variability of  $m(D)$  relationship in tropical convective clouds. Several previous studies have shown significant variability in  $m(D)$  power law including pre-factor and exponent for different flights of one and the same aircraft campaign (McFarquhar et al. 2007; Heymsfield et al. 2010). Concerning the crystal growth by pure vapor diffusion it is well known that the crystal habit is primarily a function of temperature and supersaturation. (Bailey and Hallett 2004, 2009; Kobayashi 1993). Collision growth processes (aggregation and riming) in dynamically more active clouds tremendously complicate the resulting crystal habit and associated properties (crystal geometry, density, optical properties). Therefore, and to improve our understanding of microphysical processes in clouds in general, it is necessary to get a more realistic description of ice crystals and particularly a description of their mass as a function of their size (Schmitt and Heymsfield 2010). Cloud observations are often related to radar measurements or satellite observations. The forward modeling of the remote sensing signal (active or passive) and the retrieval of cloud microphysics is linked to the model capacity to simulate the radiative transfer through a population of ice crystals of complex habits.*

*Numerous previous studies already related cloud radar reflectivity (usually at a frequency of 94GHz or 35GHz) and in-situ measurements of cloud microphysical properties. For instance in Protat et al. (2007), Hogan et al. (2006), and Pokharel and Vali (2011) the total water content is calculated assuming a constant mass-size relationship for all clouds. Derived Z-CWC relationships often need a correction which is a function of temperature. This somewhat translates the lack of knowledge of the temperature dependency of mass size relationships.”*

2. Presentation of method/results: Sections 3 and 4 should be swapped around. Section 4 currently is heavy on methodology and its result, its linear relationship between beta and sigma, will help focus section 3 and understanding of the results in that section. Since the remainder of the results concern beta\_sigma, the authors should consider

ignoring the use of beta\_i on pages 2992 and 2993. Although interesting, the beta\_i do not re-appear once the beta\_sigma have been introduced. The discussion on pages 2992 and 2993 could be shortened and focus on the derivation of alpha\_sigma.

*According to the reviewer's recommendations we suggest merging sections 3 and 4. We'd like to keep sections 4.1 and 4.2 which would become 3.1 and 3.2. A section 3.3 would be a reduced version of the entire current section 3. This section 3.3 would focus on the calculation of the mass-size relationship starting from  $\beta_\sigma$  deduced from the equation 11. Figure 4 will be deleted. Figures 2 and 3 will be directly followed by figure 8 (current numbering). Then we wish to keep an explanation on the evaluation of the uncertainty of the retrieval method itself (without counting the uncertainties from PSD, shattering impact, etc....). This part will be illustrated without the  $\alpha_i$  and  $\beta_i$  coefficients, to make the reading of this paper easier.*

### « 3.3 Mass-diameter coefficients and CWC retrieval

*In order to better understand the importance of coefficients  $\alpha$  and  $\beta$  in eq. 1 and their impact on the retrieved CWC, reflectivity simulations at 94GHz have been performed and compared with corresponding measured reflectivities on the flight trajectory. Simulations of radar reflectivities are complex when considering non-spherical ice crystals. In this study, the backscatter properties of the hydrometeors have been simulated with the T-matrix method (Mishchenko et al. 1996) for crystals and/or with Mie theory for spherical particles. In order to model the scattering properties of the ice particles, these particles are assumed to be oblate spheroids with a flattening that equals the mean aspect ratio  $\overline{As}$  of the hydrometeors with  $D_{max} < 2mm$ , which mainly impact the simulated reflectivity:*

$$\overline{As} = \sum_{D_{max}=55\mu m}^{200\mu m} Pi(D_{max}) \cdot As(D_{max}) \quad (4),$$

where

$$Pi(D_{max}) = \frac{N(D_{max}) \cdot D_{max}^3 \cdot \Delta D_{max}}{\sum_{D_{max}=55\mu m}^{200\mu m} N(D_{max}) \cdot D_{max}^3 \cdot \Delta D_{max}} \quad (5).$$

*$N(D_{max})$  is the concentration of the hydrometeors and  $As(D_{max})$  their average aspect ratio.  $\overline{As}$  is calculated every 5 seconds as is done for the composite PSD. Of course at 94GHz the hydrometeors with  $D_{max} > 2mm$  are not invisible, but the increase of their backscattering cross section ( $Q_{back}$ ; Fig. 2) as a function of their size is not sufficient taking into account the very small crystal concentrations beyond a few millimeters. Thus, their impact on the simulated reflectivity is negligible. Fig. 2 also shows the impact of  $As$  on the effective reflectivity for 94 GH, for varying  $As$  between 0.5 and 1. For  $As = 1$  Mie theory was applied. For diameters less than 600-900  $\mu m$  simulated radar reflectivities agree well with those calculated using the Rayleigh approximation. As can be seen in this figure, the so-called 'Mie*

effects' appear only for larger diameters and decreasing aspect ratio  $As$ . The  $Pi(D_{max})$  weighting function impacts the mean aspect ratio  $\overline{As}$  which will be used to constrain the  $T_{matrix}$  simulations of the radar reflectivity. In  $Pi(D_{max})$  the maximum length of hydrometeors is taken at its third order, to take into account the impact of the hydrometeors in the sampling volume. This choice is a compromise to accomplish for the lack of knowledge to constrain the variability of  $Q_{back}$  for natural ice crystals, and previous approximations using the Mie solution to model the  $Q_{back}$ . Instead of the third order of  $D_{max}$ , we could have chosen the number concentration  $N(D_{max})$  or  $N(D_{max}) \cdot S(D_{max})$ , both may overestimate the smaller ice crystals, while  $D_{max}^6$  (Rayleigh approximation) does not seem to be the best choice either in this context. To quantify the impact of the uncertainty to the calculation of  $\overline{As}$  on the retrieved CWC, it has been calculated that (with respect to  $Pi(D_{max})$  defined in equation (5), CWC increases by about 12% if  $Pi$  is calculated from  $N(D_{max})$ , and CWC increases by about 6% if  $Pi$  is calculated from  $N(D_{max}) \cdot S(D_{max})$ .

In general, we assume that hydrometeors consist of a homogeneous mixture of ice and/or air. Their dielectric properties of the particles are therefore a function of the mass-diameter relationship that represents the fraction of ice  $f_{ice}$  (equation 6) in the hydrometeors. Equation 6 explains how the ice fraction of the solid hydrometeor are calculated, with  $\rho_{ice} = 0.917 \text{ g cm}^{-3}$ . The ice fraction  $f_{ice}$  cannot exceed 1.

$$f_{ice} = \min \left( 1, \frac{\alpha \cdot D_{max}^{\beta}}{\frac{\pi}{6} \cdot \rho_{ice} \cdot D_{max}^3} \right) \quad (6).$$

Once  $f_{ice}$  is determined the refractive index is calculated using the approximation of Maxwell Garnet (1904). The mass of the spheroid does not depend on the aspect ratio  $As$ , but the backscattering properties do. By means of the  $T$ -matrix method the backscattering coefficient of a particle is calculated assuming the particle volume as a prolate spheroid with a diameter  $D_{Tmatrix}$ :

$$D_{Tmatrix} = D_{max} \cdot \sqrt[3]{\frac{1}{As}} \quad (7)$$

In order to calculate the 94 GHz radar reflectivity, the particle number distribution  $N(D_{max})$ , its mean aspect ratio  $As$ , and the ice fraction  $f_{ice}$  of the hydrometeors, also the coefficients  $\beta$  and  $\alpha$  of the mass-diameter relation (eq. 1) must be given. Fig. 3 gives an outline of the technique developed to retrieve the  $m(D)$  coefficients. After imposing  $\beta_{\sigma}$  the prefactor  $\alpha_{\sigma}$  is determined by minimizing the difference between the simulated and measured reflectivities. Then the corresponding CWC in  $\text{g m}^{-3}$  is calculated from the PSD and the mass-diameter coefficients:

$$CWC(\alpha_{\sigma}, \beta_{\sigma}) = 10^3 \cdot \sum_{D_{max}=50\mu\text{m}}^{D_{max}=6400\mu\text{m}} N(D_{max}) \cdot \alpha_{\sigma} D_{max}^{\beta_{\sigma}} \cdot \Delta D_{max} \quad (8).$$

Fig. 8 shows the temporal evolution of the PSD, mean aspect ratio  $\overline{As}$ , exponent  $\beta_\sigma$ , derived  $\alpha_\sigma$ , and calculated  $CWC(\alpha_\sigma, \beta_\sigma)$  for a cloud sequence of the flight 18 during MT2010. The temporal variabilities of the PSD,  $\overline{As}$ , the exponent  $\beta_\sigma$ , constrained pre-factor  $\alpha_\sigma$ , and CWC are considerable..

Uncertainty of this method, calculating CWC, is evaluated when systematically varying  $\beta$  in the interval [1;3], while for each  $\beta$  the pre-factor  $\alpha$  is deduced accordingly (by minimizing the difference between the simulated and measured reflectivities). Subsequently, corresponding CWC values are calculated. For a given time step (of 5 seconds) the calculated minimum and maximum values of CWC ( $CWC_{min}$  and  $CWC_{max}$ , respectively) are used to estimate the maximum uncertainty ( $\Delta CWC_{max}$ ) of the retrieved CWC.  $\Delta CWC_{max}$  is simply defined as the maximum difference between  $CWC(\alpha_\sigma, \beta_\sigma)$  and the largest or smallest value of CWC. This maximum uncertainty can be also calculated in terms of the relative error in percent:

$$100 \cdot \frac{\Delta CWC_{max}}{CWC(\alpha_\sigma, \beta_\sigma)} = 100 \cdot \frac{\text{MAX} ( [ |CWC_{min} - CWC(\alpha_\sigma, \beta_\sigma)| ; |CWC_{max} - CWC(\alpha_\sigma, \beta_\sigma)| ] )}{CWC(\alpha_\sigma, \beta_\sigma)} \quad (9).$$

For both measurement campaigns MT2010 and MT2011, Fig. 5 shows the distribution of  $\Delta CWC_{max}$  in percent. For most of the calculated CWC values the maximum error remains below 30%. Average values of the maximum deviations in CWC are 21% for MT2010 and 20% for MT2011, respectively.

These uncertainties do not take into account the uncertainty related to the measurements of the reflectivity by the cloud radar RASTA. Tab. 2 gives the impact of the reflectivity on the retrieved  $m(D)$  coefficient  $\alpha$ . For example, if the reflectivity is shifted by +1 dBZ to simulate a radar calibration error, the CWC retrieval is increased by 11% with respect to the CWC given by the measured reflectivity. The CWC retrieval of this method is pretty sensitive to uncertainties in measured reflectivities and also to the shape (or flattening) parameter used to simulate the radar reflectivity.”

3. Section 5: This results section is currently overflowing with figures which are poorly introduced, and various discussion points seem irrelevant to the paper’s main focus. The only results related to the section title ("Mass-diameter relationship") are figures 10 and 11b and 11c; it is unclear why the other figures are included. The authors should consider reducing this section to "Retrieved mass-diameter relationships", which discusses figures 10, 11b, and 11c. This discussion can then continue with figure 9, which compares the CWC simulated from the retrieved mass-diameter relationship with theory and observations. The remaining figures (11a, 11d-f, 12, 13, 14, 15) all show interesting results, but these have no immediate purpose in this paper. If the authors are adamant that these figures should be included, they are advised to combine them in a separate section, for instance "Altitude relationships of cloud-ice properties".

Figure 11 is modified, taking into account the comments of referee#1 and #2. In addition, figures 12 and 15 have been deleted.

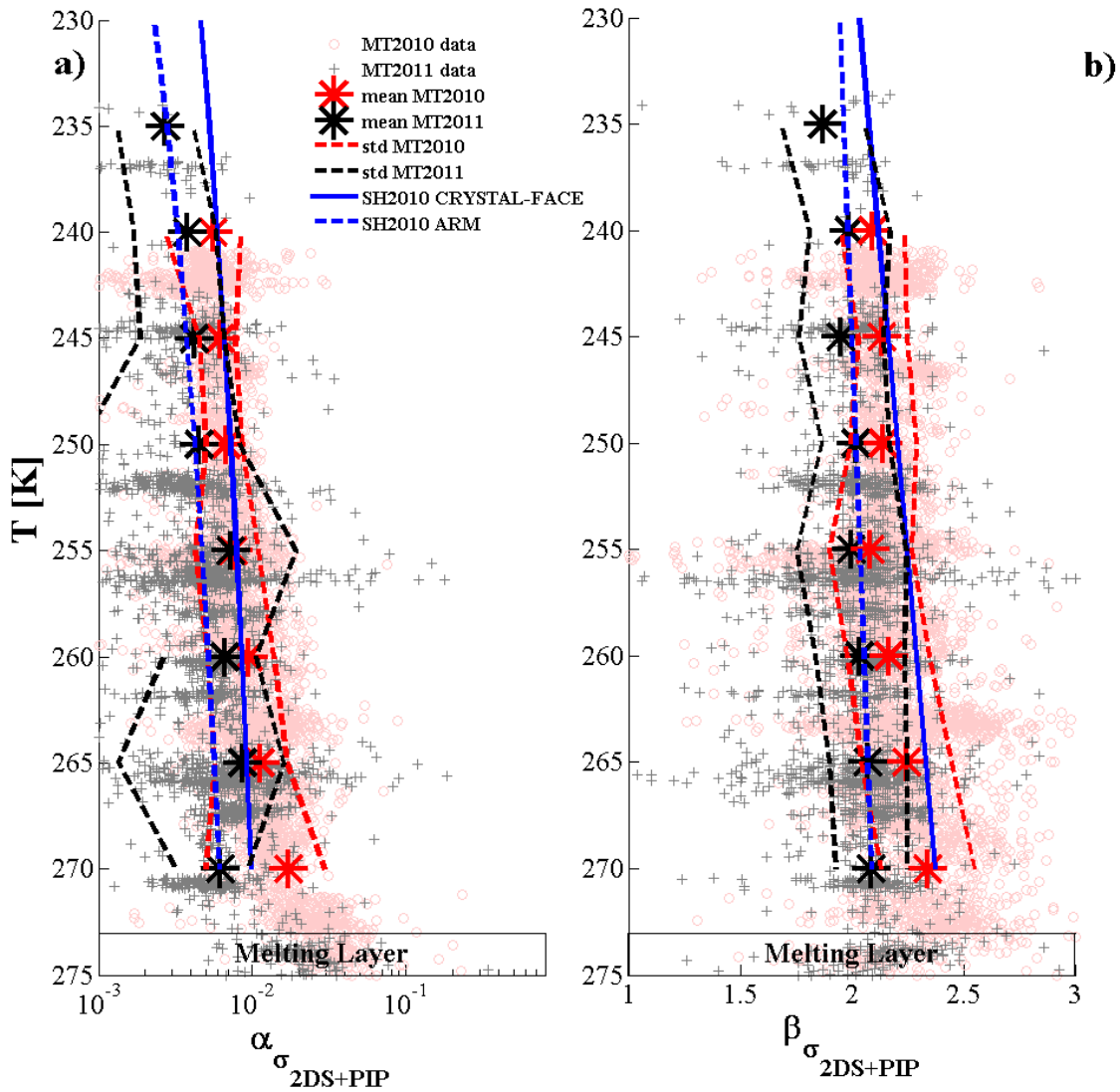


Figure 11 : Vertical profile of  $m(D)$  coefficients constrained by T-matrix and the variability of S-D exponent  $\alpha$  calculated from 2D-S plus PIP images. (a)  $\alpha_{\sigma}$  versus the temperature in K. (b)  $\beta_{\sigma}$  versus the temperature in K. Pink circle show data points (5-seconds time step) of MT2010, grey crosses show MT2011 data. Red and black stars present mean values of  $m(D)$  coefficients in 5K temperature intervals for MT2010 and MT2011, respectively. Dashed red and black lines show standard deviations of MT2010 and MT2011, respectively, from the mean value. Blue solid and dashed lines show vertical profiles of SH2010 obtained for CRYSTAL-FACE, and for ARM, respectively.

Major comments (science and method):

4. Matching of observations in time and space (pages 2989-2990): It is currently unclear over how many observations the particle size distribution is calculated; what is the stretch of time?

At the end of section 2 :

“The bin resolution of the composite distributions is given by  $\Delta D_{max}$  equal to 10 microns. Examples of PSD and TSD are presented in Fig. 1. Overall the 2 probes are in good agreement in their common size range. Fig. 1a shows the PSD composite distribution and the individual PSDs of the individual probes. The AsD composite distribution is shown in Fig. 1b. It can be seen that the transfer function smoothes the transition from the 2D-S to the PIP.

*PSD (as AsD) and RASTA reflectivity are synchronized and averaged over the same time step which is 5 seconds. RASTA reflectivities are measured in nadir and zenith of the flight trajectory and interpolated to the flight level. Interpolation is made ...”*

And what is  $L^{-1}$  (line 9, pages 2989)?

*Total hydrometeor concentrations are given per liter, concentrations in PSD are given per liter and per micrometer.*

The authors should include a paragraph at the end of section 2 to describe the radar data: how are the radar observations matched in time and space to the PSD detected by the aircraft? This currently partly appears elsewhere but the information is required here for the reader.

*See answer above presented to respond to “Major comments (science and method):”*

5. Equation 4 (mean aspect ratio): At a later stage, the authors mention that  $\langle As \rangle$  is calculated only for  $D_{max}$  within the 94GHz radar sensitivity - is this true for equation 4 as well? If so, please adjust this in the summation. Since the mean aspect ratio is used for radar reflectivity calculations, it is worrying that the summation is weighted by particle number concentration, and not by mass or mass-squared. The radar reflectivity will be dominated by large particles, so the effect of flattening observed in Z should mostly come from large particles. The  $\langle As \rangle$  however is weighted towards the more numerous (likely smaller) particles, which are expected to be more spherical, thus  $\langle As \rangle$  might be closer to 1 than what would be observed by the radar. Could the authors consider changing the equation to weight it with mass or mass-squared instead of number, or at the very least consider this option in the text?

*See answer above presented to respond to the first part of the 2<sup>nd</sup> point of the reviewer’s “Major comments (structure):”*

6. Vertical trends of mass-diameter coefficients: This appears to be only weakly supported by the results, but is stated as a major conclusion in both the abstract and the conclusions. In a revised section 5, the authors are advised to more carefully establish these "vertical trends": what is the relationship of alpha and beta individually with temperature, and how significant is this relationship? These trends look rather vertical in figures 11b and 11c and certainly within the error bounds presented.

*In the revised version of section 5 (which becomes section 4 in the revised manuscript) we will focus more on the variability of the mass-diameter relationships (see also the subsequent answer to the reviewer’s point 7). The vertical variability will be described by fitting the mean profiles as a function of the temperature.*

7. Use of a single  $m(D)$  relationship to calculate CWC (page 3003): This seems a missed opportunity to test the effect of having a variable  $m(D)$  relationship. The authors

have the tools to assume a single  $m(D)$  relationship (e.g.  $\beta=2.44$ , page 3005) and calculate a Z-CWC relationship, or even use BF95 on their observations to calculate Z-CWC. This will test how advantageous it is to have a variable relationship, rather than comparing with P2007. Using their own data to test this, the authors could possibly add a major conclusion and scientific advance to this paper.

*To answer to the reviewer's comment, different methods have been applied to calculate CWC from measured PSD (in order to use Brown and Francis  $m(D)$  relationship, PSD were also calculated as in Brown and Francis's paper such that the diameter is  $D = (Lx+Ly)/2$ ). Subsequently, CWC can be calculated for Brown and Francis, and the other methods (H2010, SH2010). Finally, for all methods Z-CWC relationships, and Z-CWC-T relationships have been deduced (fitted), taking Z from RASTA. For each method applied to both MT datasets, correlation coefficients (cc) between Z and CWC, and model errors ( $error_z$ ) as described in equation 16 (in the current version of this paper) were calculated. From this  $error_z$ , average values, median, first quartile, last quartiles and 90<sup>th</sup> percentile were calculated. As it has been suggested by the referees #1 and #3, we used the  $\square$  coefficient (exponent from S-D fitted relationships) calculated from 2DS plus PIP images to calculate  $\beta_\sigma$  and subsequently constrain  $\alpha_\sigma$ . The results are presented in table 1. Moreover, table 2 shows corresponding results when using only 2DS images to fit the  $\square\square\square$  exponent with subsequent calculation of  $\beta_\sigma$  and  $\alpha_\sigma$ .*

*The Z(CWC ;T) –Z(CWC) columns demonstrate the improvement when the temperature is parameterized in the fitted relationships between Z and CWC.*

*The main result of this study is that  $error_z$  is minimal when comparing the CWC(Z) parameterization retrieved from T-Matrix calculations of CWC and Z from RASTA radar with CWC ( $\alpha_\sigma$ ,  $\beta_\sigma$ ) calculated with the help of  $m-D$  relationships constrained by the 2D images (2D-S plus PIP on the one hand and solely 2D-S on the other hand). The CWC(Z) parameterizations fitted for the other methods and compared to CWC ( $\alpha_\sigma$ ,  $\beta_\sigma$ ) all produce significantly larger values for  $error_z$ . When taking into account the temperature in fitting Z(CWC;T) for the time resolved T-matrix method, this does not improve significantly correlations as compared to Z-CWC parameterization only. In contrast, for the other methods applied to MT2010 and/or MT2011 datasets (averaged T-matrix, H2010 (NAMMA), H2010 convectively generated, B&F, SH2010 (Crystal Face), SH2010(ARM)), the improvement is significant when the temperature is taken into account for the MT2010 dataset. For the MT2011 dataset taking into account the temperature is not sufficient to improve Z-CWC models. The MT2011 dataset seems to have more complicated microphysical processes than MT2010.*

**Tableau 1 : Error<sub>z</sub> in percent when comparing Z-CWC and Z-CWC-T relationships with CWC calculated according to different methods applied to MT2010 and MT2011 datasets. Correlation coefficients between CWC and reflectivity are given in the column denoted cc. Average errors are given in column E. Quartile, median, third quartile and**

ninetieth percentile, are given in 1/4, 1/2, 3/4 and 9/10 columns.  $\sigma$  is calculated using S-D relationships from 2DS plus PIP.

Sigma = f(2DS+PIP)													
Z(CWC)													
	MT2010						MT2011						
method	cc	E	1/4	1/2	3/4	9/10	cc	E	1/4	1/2	3/4	9/10	
Tmatrix+2D Images of OAP	0.95	25	8	16	29	52	0.94	39	13	29	48	71	
Averaged coefficients for Tmatrix	0.81	54	16	30	49	115	0.83	76	19	41	65	126	
H2010 (NAMMA)	0.81	56	16	31	51	118	-	-	-	-	-	-	
H2010 (convectively generated)	-	-	-	-	-	-	0.83	76	19	40	65	124	
Brown & Francis	0.8	60	17	33	54	126	0.82	76	20	41	67	129	
SH2010 (CRYSTAL-FACE)	0.81	56	16	30	50	114	-	-	-	-	-	-	
SH2010 (ARM)	-	-	-	-	-	-	0.84	74	18	38	62	121	

Z(CWC ;T)														Z(CWC; T) – Z(CWC)	
	MT2010						MT2011						MT2010	MT2011	
method	cc	E	1/4	1/2	3/4	9/10	cc	E	1/4	1/2	3/4	9/10			
Tmatrix+2D Images of OAP	0.95	23	7	15	26	47	0.95	37	13	26	44	67	-2	-2	
Averaged coefficients for Tmatrix	0.82	44	11	24	42	89	0.83	72	18	37	61	115	-10	-4	
H2010 (NAMMA)	0.82	43	11	23	41	87	-	-	-	-	-	-	-13	-	
H2010 (convectively generated)	-	-	-	-	-	-	0.84	72	19	37	61	115	-	-4	
Brown & Francis	0.81	43	11	23	42	87	0.84	71	18	38	63	119	-17	-5	
SH2010 (CRYSTAL-FACE)	0.81	44	11	24	43	91	-	-	-	-	-	-	-12	-	
SH2010 (ARM)	-	-	-	-	-	-	0.82	72	18	37	61	114	-	-2	

Table 2 : As table 1 but when  $\sigma$  is derived from the 2DS S-D power law.

Sigma=f(2DS)													
Z(CWC)													
	MT2010						MT2011						
method	cc	E	1/4	1/2	3/4	9/10	cc	E	1/4	1/2	3/4	9/10	
Tmatrix+2D Images of OAP	0.95	24	7	16	29	54	0.94	41	14	29	47	74	
Averaged coefficients	0.81	52	15	29	48	109	0.81	91	19	41	65	137	

Z(CWC ; T)														Z(CWC; T) – Z(CWC)	
	MT2010						MT2011						MT2010	MT2011	
method	cc	E	1/4	1/2	3/4	9/10	cc	E	1/4	1/2	3/4	9/10			
Tmatrix+2D Images of OAP	0.95	22	7	15	26	49	0.95	38	12	26	44	67	-2	-3	
Averaged coefficients	0.83	42	11	24	42	89	0.82	85	20	38	61	129	-10	-6	

Minor comments:

8. p.2986, line 24-25: "Retrieved relationship are finally used..." - by whom? By Lawson

et al.? By the authors?

*Heymsfield et al (2002) then used the retrieved  $m(D)$  relationships to compute Ka-band radar equivalent reflectivities, which are in good agreement with measured reflectivities.*

9. p.2987, line 2-3: "vertical profiles" - of what? Radar reflectivity?

*“McFarquhar et al. (2007) derived vertical profiles of  $m(D)$  relationships in the stratiform part of Mesoscale Convective Systems (hereafter MCS) above the North American continent within and below the melting layer”*

10. p.2987, line 6: What numerical simulations? Of scattering properties?

*The beginning of the sentence has been deleted.*

*“Schmitt and Heymsfield (2010, hereafter SH2010) have simulated the aggregation of plates or columns.”*

11. p.2987, line 13-16: What was the strong relationship from H10 based on? Theory, observations, simulations, something else?

*Heymsfield et al. (2010, hereafter H10) have calculated  $m(D)$  coefficients by minimizing the differences with measured CWC for different airborne campaigns. They demonstrate that a strong relationship exists between  $\alpha$  and  $\beta$  coefficients, which was mathematically demonstrated with a gamma distribution to model the PSD. Furthermore, they argue that the BF95 relationship overestimates the prefactor  $\alpha$  for stratiform clouds, whereas  $\alpha$  is underestimated for convective clouds.”*

12. p.2989, eq.2: How good is the PIP at  $D_{max} < 950$ , if it will only measure 9 pixels across?

*In the range  $[450\mu\text{m}; 950\mu\text{m}]$  the two probes 2D-S and PIP are in agreement with respect to the size of the particle. The 2D-S is very reliable up to particle sizes of  $700\mu\text{m}$ . Below  $950\mu\text{m}$  in diameter the PIP particles are taken into account with decreasing weight, in order to ensure the continuity of the composite PSD. PIP particles of 5-7 pixels have low weight as compared to the corresponding 2D-S particle images. In contrast the weight of PIP particle images increases for particles of 8-9 pixels as compared to the 2D-S. Above 9-10 pixels, the 2D-S starts to be considerably affected by the truncation of the particles. Therefore the transition from the 2D-S to the PIP is needed before.*

13. p.2991, line 21-22: The authors are advised to call  $\alpha_i$  here  $\alpha_j$ , and use  $\alpha_i$  only for the  $\alpha$  which minimizes the reflectivity difference. (Though this part of the text may be removed if the revised discussion solely focuses on  $\alpha_{\sigma}$ ).

*This part has been modified.*

*See the answer above presented to respond to the 2<sup>nd</sup> point of the reviewer’s “Major comments (structure):”*

14. p.2992-2993: Are there no error calculations for  $\alpha$ ,  $\beta$ , and CWC?

Errors on  $\alpha$  and CWC are given in table 2 and 3. An error on the calculation of  $A_s$  of about 10% would result in an uncertainty of about  $\pm 6\%$  on  $\alpha$  and  $\pm 6\%$  on CWC. In the same way, an uncertainty of 2dBZ of the measured reflectivity would result in an uncertainty of  $\pm 26\%$  on  $\alpha$  and  $\pm 26\%$  on the retrieved CWC.

Furthermore, the calculation of  $\beta$  has an uncertainty about  $\pm 11\%$ , which is the error between the  $\beta$  calculated with the linear fit and the  $\beta$  calculated through the 3D simulation (a more detailed explanation of that error is presented in the response to reviewer 3).

The uncertainty from the reflectivity differences when finding the  $\alpha_i$  could be used to weight-average CWC in equation 8.

*Simulated and measured reflectivities are identical.*

15. equation 10: It is not clear which measurements are used to find gamma and sigma.

*S-D power laws are calculated for 5-second time intervals and are synchronized with PSD and RASTA reflectivity. In order to calculate the S-D power law, we plot the mean surface of the particles (measured during 5 seconds) versus their  $D_{max}$  (figure 2) for the two probes. S-D are then fitted by a power law described by two parameters: prefactor  $\gamma$  and exponent  $\sigma$ , individually for both probes. On a log-log scale,  $\ln(\gamma)$  is the y-axis intercept, and  $\sigma$  the slope of the linear relationship such that  $\log(S) = \sigma \cdot \ln(D) + \ln(\gamma)$ .*

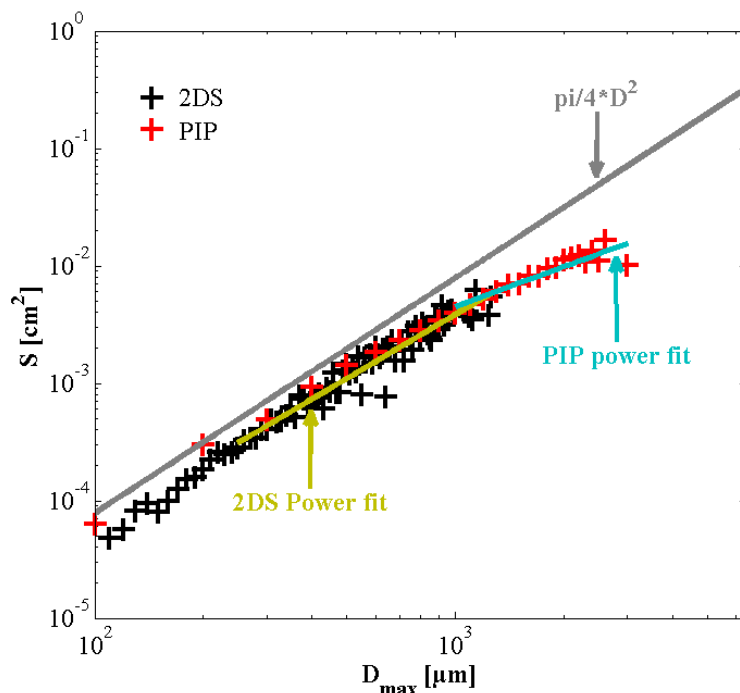


Figure 12: Mean projected surface in cm<sup>2</sup> on y-axis versus  $D_{max}$  in  $\mu\text{m}$  on the x-axis. Black symbols represent the 2DS image data and red symbols the PIP data. The grey line would be the power law fit for spherical particles. The golden line is the power law which fits the 2DS data for  $D_{max}$  larger than 250 $\mu\text{m}$  and the blue line fits the PIP data with a power law for  $D_{max}$  larger than 950 $\mu\text{m}$ .

16. equation 11: Is there any evidence in literature of such a fit? Should we expect a linear relationship between beta and sigma? A bit more discussion is required here.

*There is no evidence in literature of such a fit. SH2010 have related the fractal dimension in 2D and 3D by box counting (Falconer 2003; Mandelbrot 1982; Tang and Marangoni 2006). In this study,  $S(D)$  and  $m(D)$  relationships are studied with 3D modeled ice-crystal shapes. Then  $\sigma$  and  $\beta$  are related with the objective to preserve the variability of the  $m(D)$  exponent as a function of the 2D images recorded for the 2 campaigns (where  $\sigma$  is calculated each 5 seconds step and  $\beta$  is calculated as a function of  $\sigma$ ). The standard deviation of the model error using equation 11 is about 11%.*

*From comments of Referee #3, an additional paragraph on the uncertainty of  $\beta$  and also the impact of an eventual orientation of ice crystals during the cloud sampling has been added to the study.*

17. p.2996 lines 9-16: What type of growth speed do the authors consider? Growth in time? Growth with change in diameter?

*“In view of the results produced by the 3D simulations, it seems that  $\beta$  (and also  $\sigma$ ) does not relate much to the sphericity of the crystal shape, but more to how a population of ice crystals is growing in the 3D space (axis  $x, y, z$ ) as a function of its evolution in the direction of the maximum length.”*

18. p.2997 line 14: Where is this Sierra Nevada?

*“The data set of hydrometeors is coming from winter storms in the central Sierra Nevada in the western part of the North American continent. The crystals have been collected at the ground, and subsequently fitted to build the B&L scheme. This is not necessarily best adapted for the hydrometeor data set used in our study.”*

19. p.2997 lines 9 and 17-18: These statements appear related and should be combined in a single sentence (exponent close to 1 and good correlation).

*A good correlation between two parameters does not imply that the exponent of a power law is close to 1. An exponent close to 1 describe a linearity between to parameters, while a correlation coefficient describes to what extent two types of dataset are related.*

20. p.2998 line 5-6: Is this correlation between alpha and beta expected from theory, or is it a result of the methods used in this paper?

*For this it is a result. But it has also been demonstrated in H2010. See also answer to the comment 11.*

21. p.2998 line 14: How would the different beta-calculation of H10 affect the slope?

*Beta-calculation from fractal Dimension or by minimizing differences with a measured CWC?*

Figure 3 shows results obtained when the  $m(D)$  coefficients are calculated flight by flight thereby minimizing the differences with the retrieved mean CWC. The mean CWC has been chosen, in order to avoid biasing the findings in favor of the coefficients where  $\beta$  is constrained by the  $\sigma$  (2DS or 2DS +PIP). This is described in the current version of the paper. The huge standard deviation of  $\ln(\alpha)$  observed when we use a constant exponent  $\beta$  shows that it is important to describe variability of  $\beta$  in space and time.

Since it has been decided that the discussion of solutions of  $(\alpha_i, \beta_i)$  and  $CWC(\alpha_i, \beta_i)$  is no longer discussed in the current version of the manuscript, the study of the variability of the  $m(D)$  coefficients is tackled with the variability of Z-CWC and Z-CWC-T parameterizations for different methods of retrieved  $m(D)$  and thus CWC. The below figure will not be taken into consideration in the revised manuscript.

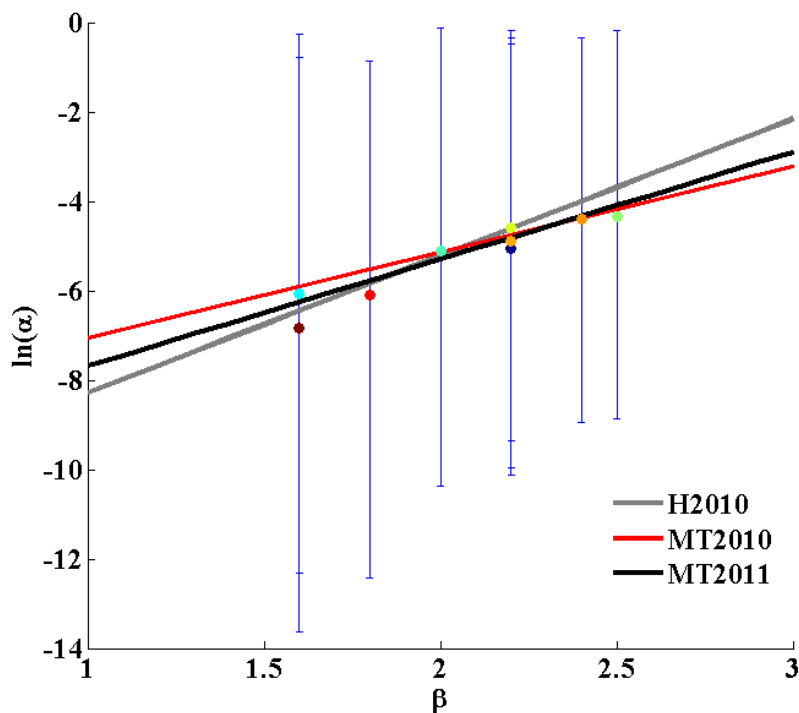


Figure 13:  $m(D)$  coefficients are obtained by minimizing differences with a the retrieved CWC. Red to orange points are obtained for MT2011. Blue to green points are obtained for MT2010. The grey line represents the results shown by H2010 for convective clouds with  $\alpha=1.17 \cdot 10^{-5} \cdot \exp(3.066 \cdot \beta)$ . The red line represents results obtained for MT2010 using the coefficient  $\alpha_\sigma$  and  $\beta_\sigma$  with  $\sigma$  calculated from the PIP plus 2DS images, with  $\ln(\alpha_\sigma)=1.9211 \cdot \beta_\sigma-8.9831$ . The black line is identical to the red line but for MT2011, with  $\ln(\alpha_\sigma)=2.396 \cdot \beta_\sigma-10.095$ . Error bars represent the first quartile and the last quartile of  $\ln(\alpha)$  for each flight.

22. p.2998 line 17: How does this (weak) variation with temperature relate to CWC(Z,T) relationships?

See answer of the 7 question in “Major Comments (science and method)”.

23. equation 12: Why not use a single exponent for the constant and the beta-dependence?

We simply wanted to keep explicitly the dependency of  $\alpha_\sigma$  from  $\beta_\sigma$ , since  $\beta_\sigma$  is calculated from fitted  $\square$ .

24. p.2999 line 17: What is this horizontal variability? Horizontal across the width of an anvil?

*In general, flight at constant levels were performed in the anvil as close as possible and parallel to the convective line for MT2010. For MT2011 flight pattern were performed downstream the convective cell, but not crossing the most active part.*

25. equation 13: Note that this equation is very similar to that for  $f_{ice}$ , that is,  $\rho_{eff} = \rho_{ice} * f_{ice}$ . Any reason why?

*This part has been completely removed to take into account the comment 3 in the “Major Comments (structure)”.*

26. p.3001 line 12-13: "most of the total mass resides in the range" - This is a confusing statement, as the total mass referred to here is actually the sum of  $M(D_{max})$  over the different  $D_{max}$ , whereas the authors have already defined  $M(D_{max})$  to be total mass. Better to define  $M(D_{max})$  as the mass of particles of size  $D_{max}$ , not as "total mass".

*This part has been completely removed to take into account the comment 3 in the “Major Comments (structure)”.*

27. p.3002: How do the authors' findings relate to existing CWC-Z relationships, and why do they think there is no CWC-Z-T relationship?

*In the initial manuscript version, the \$Z-CWC-T\$ could not be modeled with linear or quadratic functions as it is shown in the literature. After the final corrections of the RASTA dataset (details are given below this paragraph), \$Z-CWC-T\$ can be modeled. However, as is demonstrated in the answer to comment 7 of “Major comment (science and method)”, the temperature in the \$Z-CWC\$ relationships does not add significant improvements.*

*Mass-diameter relationships are calculated in this study with the help of measured reflectivity at 94GHz. Subsequently \$CWC\$ can be calculated from PSD and  $m(D)$ . Most recently the international HAIC-HIWC campaign which took place during January- March 2014 out of Darwin allowed to confront the radar reflectivities of the RASTA radar and the direct measurements of the IWC using the IKP (isokinetic evaporator probe). This confrontation allowed to improve the method correcting the radar reflectivity close to the aircraft within 900m below and above the aircraft.*

*We integrated into our answers to the reviewers and in the new version of the radar RASTA data these results taking into account the corrections of the reflectivity of RASTA in the vicinity of the aircraft.*

Is this because the temperature dependence is incorporated in alpha and beta, which both affect CWC and Z? (also p.3004, line 9-16).

*For MT2010, the variability of  $m(D)$  coefficients somewhat implicitly takes into account the temperature dependency in CWC-Z parameterizations, most likely due to the horizontal homogeneity of cloud microphysics..*

*For MT2011 the microphysical processes seem to be more complicated to be better parametrized if temperature is incorporated in the parametrisation (CWC-Z-T).*

28. p.3005 line 4-5: Is there any significance in the MT2010 and MT2011 sharing the same beta?  
 How do these average alpha and beta compare with literature?

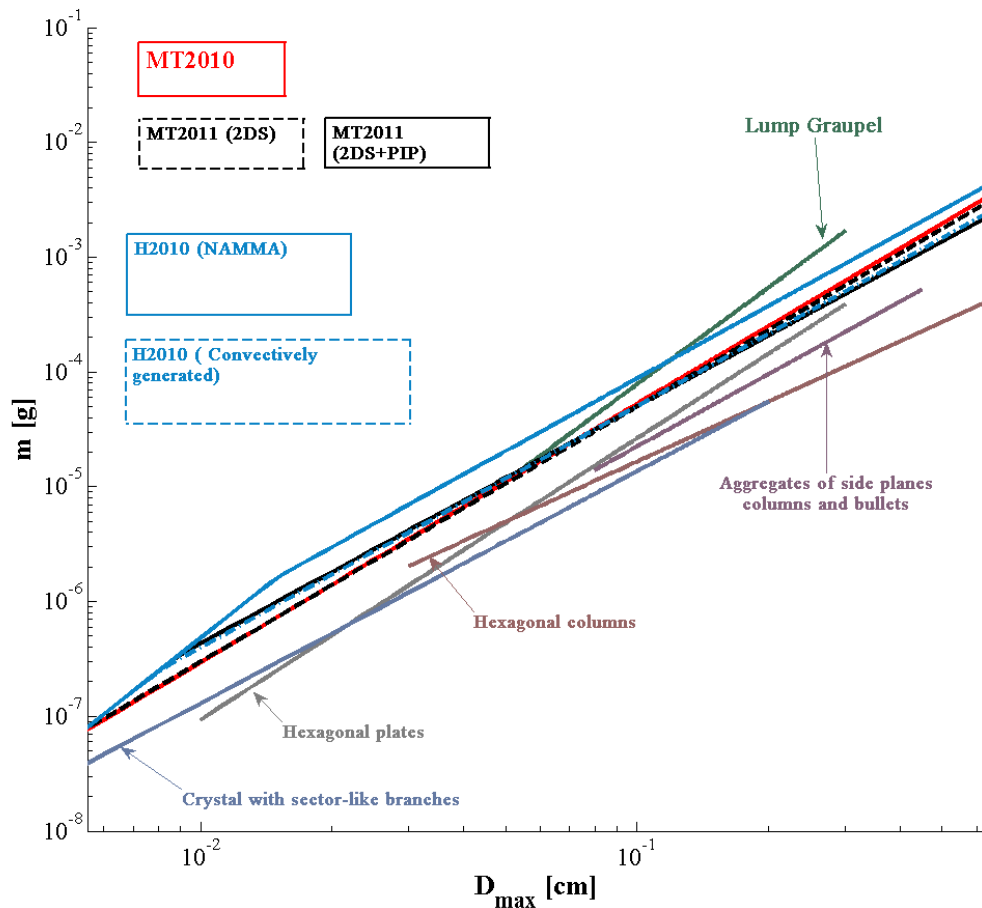


Figure 14 : Mass of ice crystals in gram on y axis, as a function of their  $D_{max}$  in cm on the x axis. The red line represents mean values of  $m(D)$  coefficients for MT2010 when  $\sigma$  is determined from 2D-S plus PIP images with  $\alpha=0.0098$  and  $\beta=2.26$ . Likewise, the black dashed line represents  $m(D)$  coefficients for MT2011 with  $\alpha=0.0057$  and  $\beta=2.06$ . The black line represents MT2011 when  $\sigma$  is determined from 2DS only with  $\alpha=0.0082$  and  $\beta=2.22$ . The blue line represents  $m(D)$  coefficients taken from H2010 for the NAMMA campaign with  $\alpha=0.011$  and  $\beta=2.1$ . Dashed blue line stands for H2010, but for convectively generated systems with  $\alpha=0.0063$  and  $\beta=2.1$ . Blue grey line is given by Mitchell 1996 for crystal with sector-like branches with  $\alpha=0.00142$  and  $\beta=2.02$ . Grey line (Mitchell 1996) represents hexagonal plates with  $\alpha=0.00739$  and  $\beta=2.45$ . Brown grey line (Mitchell 1996) represents hexagonal columns with  $\alpha=0.000907$  and  $\beta=1.74$ . Purple grey line (Mitchell 1996) is for aggregates of side planes columns and bullets with  $\alpha=0.0028$  and  $\beta=2.1$ . Green line (Mitchell 1996) is for Lump Graupel with  $\alpha=0.049$  and  $\beta=2.8$ .

*Averaged values of  $m(D)$  coefficients found for MT2010 and MT2011 with  $\sigma$  determined from 2DS only are relatively close. They give less mass for a same  $D_{max}$  if they are compared with  $m(D)$  coefficients of H2010 for NAMMA. Average values for  $m(D)$  coefficients when 2DS plus PIP are used to determine  $\sigma$ , show similar trends between H2010 for cloud convectively generated and MT2011.  $m(D)$  coefficients given by Mitchell 1996 give less mass for a same  $D_{max}$  compared with the  $m(D)$  relationships cited before, with an exception for the lump graupel's  $m(D)$  coefficients which give largest mass for particles beyond 1mm compared to all the other  $m(D)$  relationships. Mitchell's lump graupel still give larger mass for particles beyond 500 $\mu$ m compared to MT2010 and MT2010  $m(D)$  from T-matrix and H2010 convectively generated  $m(D)$ .*

*Note that for MT2010 when using the 2DS plus PIP to determine  $\square$  we find  $m(D)$  coefficients close to those found with 2DS with  $\alpha=0.0093$  and  $\beta=2.25$*

29. p.3005 line 10-11: "Since  $\langle A_s \rangle$  increases with altitude, the reflectivity of the larger diameter particles decreases with altitude" - a large particle's reflectivity will change with altitude if its own  $A_s$  increases with altitude, not necessarily the mean  $A_s$ . The mean  $A_s$  could simply change because there are more numerous small (spherical) ice particles. The current statement is confusing and should be rewritten.

*This section has been deleted since the corresponding figure has been removed, as proposed in the comment 2 of "Major comments (Structure)".*

30. Figure 16: What is the purpose of this figure and why is it introduced at this stage? Its discussion on p.3005-3006 reads as a description of observations and would have made more sense in section 2.

*See also referee #1 specific comments.*

*"Next to the Doppler Cloud radar RASTA (Protat et al. 2009) in-situ measurements of microphysical properties were performed using a new generation of optical array probes (OAP): the 2-D stereo probe (2DS) from Stratton Park Engineering Company (SPEC) Inc. which allows to monitor 2D images in the size range 10-1280 $\mu$ m, and the Precipitation Imaging Probe (PIP) from droplet Measurement Technologies (DMT) which measured hydrometeors in the size range from 100-6400  $\mu$ m. Figure 16 (in the first manuscript version) summarizes the observations of typical crystal morphologies observed during the 2 campaigns. 2D images are presented as a function of altitude. On the left side of Fig. 16 hydrometeors observed in continental MCS are shown, whereas on the right side hydrometeors observed in oceanic MCS are presented. In the two first levels (-1°C and -5°C) hydrometeors are similar with one exception. For others levels ice crystal shapes are in general different. Observations of significant amounts of dendrites (which typically develop due to water vapor diffusion only) occurred in MT2011, while 2D images for MT2010 generally look more like aggregates and graupels."*

### Comments of referee #3.

1. The authors state that their work was partially inspired by the work of Schmitt and Heymsfield 2010. While there are substantial similarities in some of the particle probe simulations, the work by Schmitt and Heymsfield did not use any remote sensing data. The authors of this work state that Schmitt and Heymsfield used remote sensing data from ARM to constrain the relationship between alpha and beta. The ARM data presented were another aircraft particle probe dataset. The authors should re-read the right column on page 1612 of Schmitt and Heymsfield to understand how the alpha factor was mathematically (not empirically) determined in that study.

*“Schmitt and Heymsfield (2010, hereafter SH2010) have simulated the aggregation of plates and columns. Fractal 2D and 3D analyses calculated from the box counting method (Tang and Marangoni 2006) stated that the fractal coefficient in the 3D space is equal to  $\beta$ . This allowed to derive a relationship that calculates the exponent  $\beta$  from the 2D fractal dimension of the 2D images. Once  $\beta$  has been fixed, the pre-factor  $\alpha$  is calculated from the area measurement.”*

I would also encourage the authors to try this method and see how it compares to their alpha values.

*In our study presented, it is not stated that  $\beta$  is equal to the fractal dimension in the 3D space. Of course, we would be interested working with the authors of SH2010 to make a separate study on the comparison of our 2 methods. The comparison is beyond the scope of this study.*

2. The authors state that they only used the 2DS probe for area dimensional relationships even though PIP data was available. How much difference was there between 2DS and PIP area measurements at the largest sizes that the 2DS was seeing? There will obviously be discrepancies at small (for the PIP) sizes, but there shouldn't be too much difference at larger sizes (more than 20 pixels for the PIP).

*In general, differences between the mean projected surface from 2DS images and from PIP images within the overlapping size range do not show large discrepancies (figure 1).*

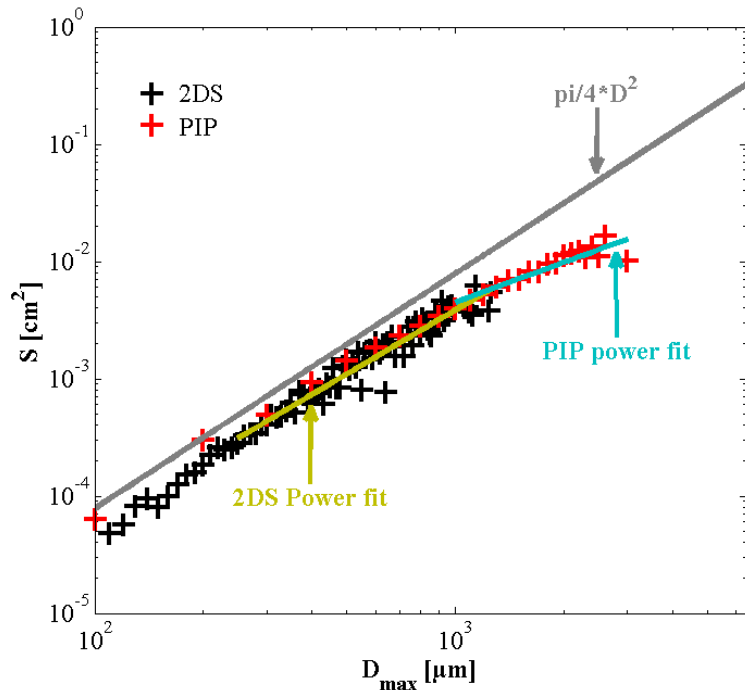


Figure 1 : Mean projected surface in cm2 on y-axis versus Dmax in μm on the x-axis. Black symbols represent the 2DS image data and red symbols the PIP data. The grey line would be the power law fit for spherical particles. The golden line is the power law which fits the 2DS data for Dmax larger than 250μm and the blue line fits the PIP data with a power law for Dmax larger than 950μm.

My concern is that in not using the PIP area information for the largest sizes, you may be losing valuable information on the fractal properties of the particle population. The density values determined for large particles suggest that there should be a lot of graupels or hail present, and it is likely that the PIP would show that better.

See also our detailed answer on similar referee #1 comments.

Shortly, we now introduced a 2D-S plus PIP common  $\sigma$  exponent taking into account the 2DS and PIP 2D images. This  $\sigma$  exponent is calculated by weighting the two  $\sigma$  that are derived separately for 2D-S and PIP images, respectively, with the ratio of the surface covering the size range where each (for 2D-S and for PIP) S-D relationship has been calculated:

$$\sigma = \frac{\sum_{D_{\max}=250\mu\text{m}}^{950\mu\text{m}} N(D_{\max}) \cdot S(D_{\max})}{\sum_{D_{\max}=250\mu\text{m}}^{6450\mu\text{m}} N(D_{\max}) \cdot S(D_{\max})} \cdot \sigma_{2DS} + \frac{\sum_{D_{\max}=950\mu\text{m}}^{6450\mu\text{m}} N(D_{\max}) \cdot S(D_{\max})}{\sum_{D_{\max}=250\mu\text{m}}^{6450\mu\text{m}} N(D_{\max}) \cdot S(D_{\max})} \cdot \sigma_{PIP}$$

Also note, that aircraft probe data at large particle sizes aren't necessarily randomly oriented. This could affect your results as well. Larger particles are naturally oriented due to aerodynamic affects and this orientation may not be disturbed enough by the airflows near the probe for the orientation to be considered random.

For sure, the eventual orientation of particles during the measurement influences the resulting power laws (figure3). The fact that in our theoretical simulations, orientation is not

*avored, involves that all the orientations are equally possible. However, there is no study concerning an eventual orientation of particles during their recording with cloud probes mounted on the Falcon wing stations. To quantify this uncertainty, we may take for a given calculated mass of a crystal its minimum  $D_{max}$  (which will be an underestimation with respect to its real value) and a maximum  $D_{max}$  (close to the real value) calculated with respect to the real  $D_{max}$ . By modeling both types of projected  $D_{max}$  according to the crystal mass and doing this for all simulated shapes, we obtain an uncertainty related to the projection of possibly oriented 3D hydrometeors projected on a 2D plane (figure 4).*

*The model error has a standard deviation of 11%, which is the error between the  $\beta$  calculated with the linear fit and the  $\beta$  calculated through the 3D simulation. For  $\ln(\alpha)$  the model error has a standard deviation of 70%. By the way, this latter large error is the reason why the results obtained for pre-factors with the 3D simulations cannot be used.*

Simulations of Hexagonal Columns such  $L=0.2*H$

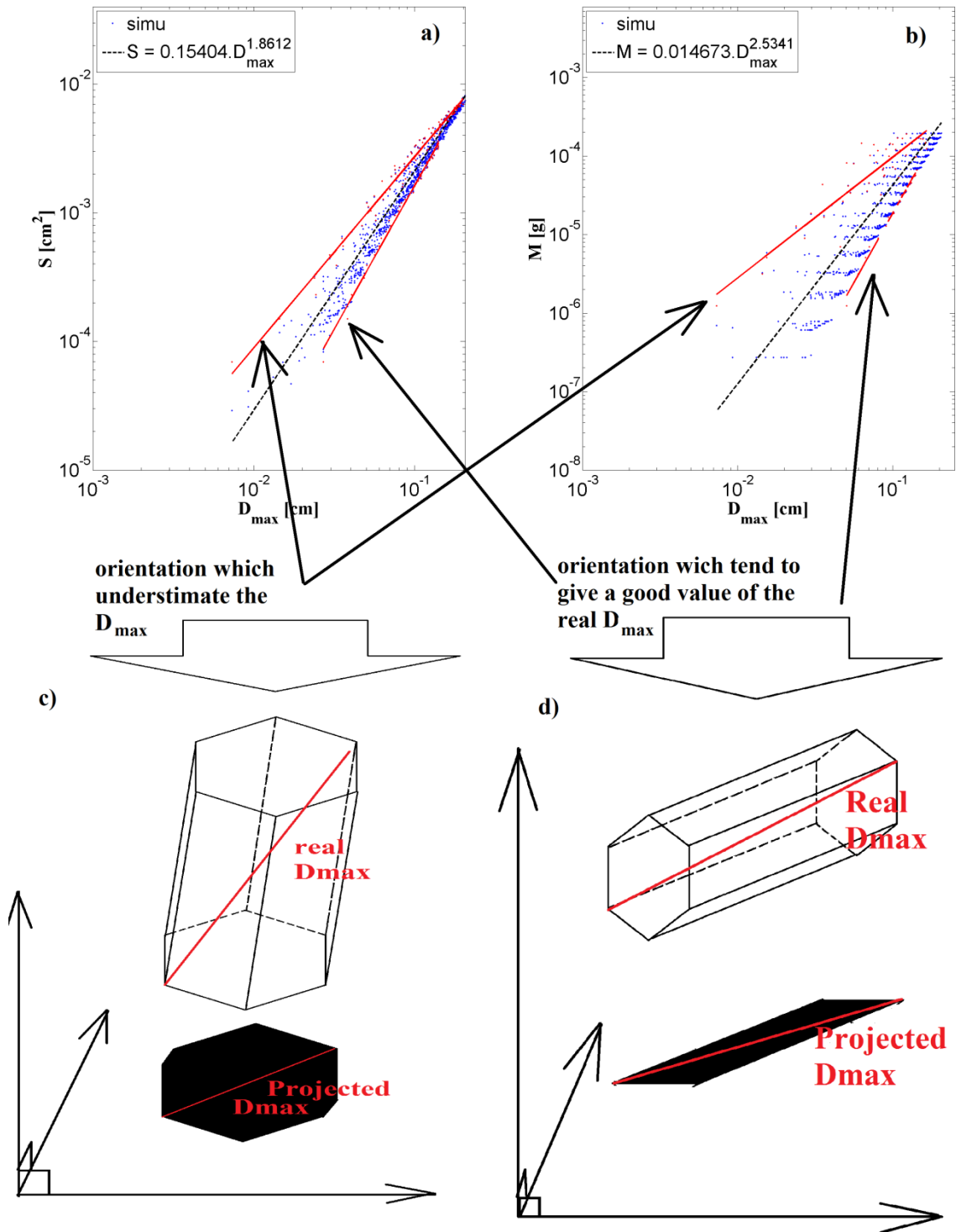


Figure 15 : Exemplary results obtained for a 3D simulation of columns characterized by  $Length=0.2*Height$ . a)  $S(D)$  plot: Blue points are the simulated data for the column, red lines are power law fits enclosing most of the data points for all possible orientations. The dashed black line is the mean of the two power laws (= the mean between two red lines when the orientation underestimates  $D_{max}$  and when the orientation is close to the real  $D_{max}$ ). b)  $m(D)$  plot: same as for a) but with the mass of the simulated columns which is now on the y-axis; c) schematic of a 3D shape oriented in the 3D space when its orientation gives an underestimated value of the real  $D_{max}$  of the ice crystals. d) Schematic of a 3D shape oriented in the 3D space when its orientation gives a close value of the real  $D_{max}$  of the ice crystals.

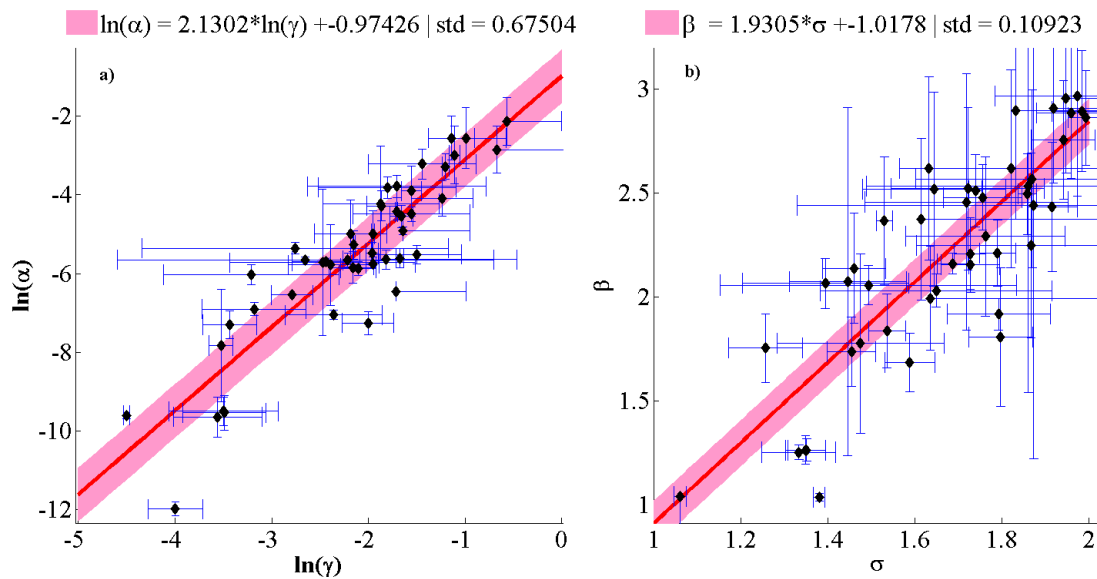


Figure 16 : Black symbols are data points for single 3D habits. Error bars give the uncertainty due to the orientation of the ice crystals during arbitrary projection on 2D plane. Red line is the linear fit between the corresponding S(D) coefficients and the m(D) coefficients. The pink band takes into account the standard deviation of the error between the fit and the modeled values. a) is for pre-factors and b) is for the exponents.

3. The choice of mostly pristine particle shapes for use in determining the relationship between the power is not really realistic. The shapes that you show in figure 6, how often do you see these shapes in the 2DS data or, more important, in the PIP data? This is probably part of the reason that your equation 11 is so substantially different from the results found in Schmitt and Heymsfield.

*In SH2010, the study is only reported on aggregates of columns and plates. Our study wants to cover the maximum of different habits. Now, in addition and according to this reviewer's comment, additional simulations with various kinds of aggregates have been added to this study. These new simulations are also integrated to the figure 3 below. Accordingly, figure 7 of the current version of the manuscript is updated.*

*Table 4 is also updated to take into account the added habit types resembling aggregates and corresponding results.*

*Then figure 6 of the current version is updated in order to take into account reviewer#1 comments.*

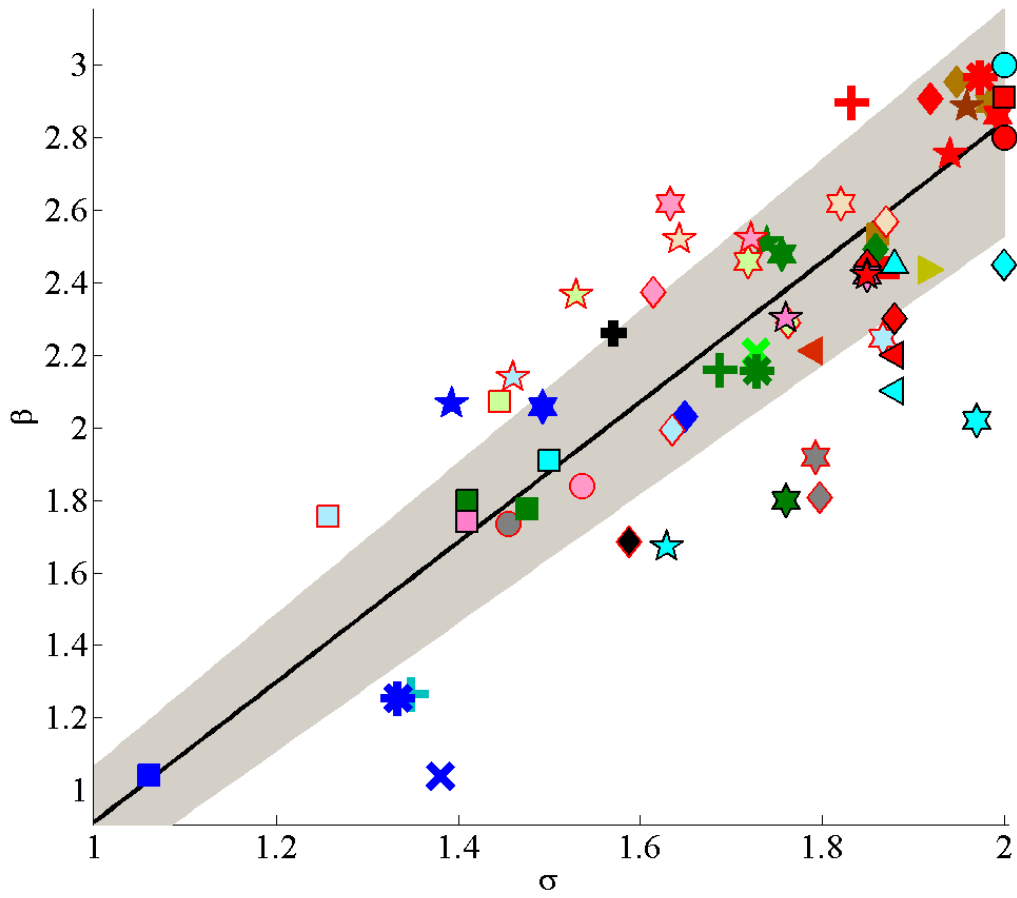


Figure 17 : Exponent  $\beta$  of  $m(D)$  relationships as a function of the exponent  $\sigma$  of the respective  $S(D)$  relationships. Each data point either with red contours or without contours is deduced for a population of 1000 simulated 3D shapes and corresponding projections. Symbols with red contours are deduced for 3D aggregates of crystals of an elementary shape. Symbols with black contours stem from Mitchell (1996). The legend for symbols is given in table 4. A linear fit of all simulated data is shown by the black line. The grey band gives the mean standard deviation of 11%.

Table 3: Ice crystal types and corresponding exponents ( $\sigma$ ) and ( $\beta$ ) of  $S(D)$  and  $m(D)$  relations, respectively. The symbols in the left column are subsequently used in Fig. 8 for individual ice crystal shapes. The first part of the table stems from Mitchell (1996) where random orientation is assumed for particles with  $D_{max} < 100\mu\text{m}$ , whereas for particles beyond  $100\mu\text{m}$  horizontal orientation is assumed. The second part of the table stems from simulations.

symbol	Description	Range	$\sigma$	$\beta$
<b>Ice crystal shapes from Mitchell (1996)</b>				
	hexagonal plates	$15\mu\text{m} < D_{max} < 100\mu\text{m}$	1.85	2.45
	hexagonal plates	$100 < D_{max} < 3000\mu\text{m}$	2	2.45
	hexagonal columns	$30 < D_{max} < 100\mu\text{m}$	2	2.91
	hexagonal columns	$100 < D_{max} < 300\mu\text{m}$	1.5	1.91
	hexagonal columns	$D_{max} > 300\mu\text{m}$	1.41	1.74
	rimed long columns	$200 < D_{max} < 2400\mu\text{m}$	1.41	1.8
	crystals with sector-like branches (P1b)	$10 < D_{max} < 40\mu\text{m}$	1.85	2.42
	crystals with sector-like branches (P1b)	$40 < D_{max} < 2000\mu\text{m}$	1.97	2.02
	broad-branched crystals (Plc)	$10 < D_{max} < 100\mu\text{m}$	1.85	2.42
	broad-branched crystals (Plc)	$100 < D_{max} < 1000\mu\text{m}$	1.76	1.8
	stellar crystals with broad arms (P1d)	$10 < D_{max} < 90\mu\text{m}$	1.85	2.42
	stellar crystals with broad arms (P1d)	$90 < D_{max} < 1500\mu\text{m}$	1.63	1.67
	densely rimed dendrites (R2b)	$1800 < D_{max} < 4000\mu\text{m}$	1.76	2.3
	side planes (S1)	$300 < D_{max} < 2500\mu\text{m}$	1.88	2.3
	bullet rosettes, 5 branches at $-42^\circ\text{C}$	$200 < D_{max} < 1000\mu\text{m}$	1.57	2.26
	aggregates of side planes	$600 < D_{max} < 4100\mu\text{m}$	1.88	2.2
	aggregates of side planes, columns & bullets (S3)	$800 < D_{max} < 4500\mu\text{m}$	1.88	2.1
	assemblies of planar polycrystals in cirrus clouds	$20 < D_{max} < 450\mu\text{m}$	1.88	2.45
	lump graupel (R4b)	$500 < D_{max} < 3000\mu\text{m}$	2	2.8
	hail	$5000 < D_{max} < 25000\mu\text{m}$	2	3
<b>Simulations of Ice-Crystals shape</b>				
	columns ( $H=5*L$ )	$100 < D_{max} < 1000\mu\text{m}$	1.86	2.53
	columns ( $H=10*L$ )	$100 < D_{max} < 1000\mu\text{m}$	1.87	2.44
	columns ( $L=160\mu\text{m}$ )	$100 < D_{max} < 1000\mu\text{m}$	1.06	1.04
	columns ( $L = \sqrt{H}$ )	$100 < D_{max} < 1000\mu\text{m}$	1.48	1.78
	thick star ( $H = 0.2*L$ )	$200 < D_{max} < 1200\mu\text{m}$	1.98	2.89
	thick star ( $H = 0.1*L$ )	$200 < D_{max} < 1200\mu\text{m}$	1.99	2.86
	thick stars ( $H=40\mu\text{m}$ )	$200 < D_{max} < 1200\mu\text{m}$	1.49	2.06
	thick stars ( $H = \sqrt{L}$ )	$200 < D_{max} < 1200\mu\text{m}$	1.76	2.48
	thin stars ( $H=0.2*L$ )	$100 < D_{max} < 1000\mu\text{m}$	1.96	2.89
	thin stars ( $H=0.1*L$ )	$100 < D_{max} < 1000\mu\text{m}$	1.94	2.75
	Thin stars ( $H=40\mu\text{m}$ )	$100 < D_{max} < 1000\mu\text{m}$	1.39	2.06
	thin stars ( $H = \sqrt{L}$ )	$100 < D_{max} < 1000\mu\text{m}$	1.74	2.51
	plates ( $H= 0.2*L$ )	$200 < D_{max} < 2000\mu\text{m}$	1.95	2.96
	plates ( $H = 0.1*L$ )	$200 < D_{max} < 2000\mu\text{m}$	1.92	2.91
	plates ( $H=40\mu\text{m}$ )	$200 < D_{max} < 2000\mu\text{m}$	1.65	2.03

	plates ( $H = \sqrt{L}$ )	$200 < D_{max} < 2000 \mu\text{m}$	1.86	2.49
	rosettes ( $L = 50 \mu\text{m}$ ; $N_{max} = 3$ )	$50 < D_{max} < 500 \mu\text{m}$	1.37	1.04
	rosettes ( $L = \sqrt{H}$ ; $N_{max} = 3$ )	$50 < D_{max} < 500 \mu\text{m}$	1.69	2.21
	rosettes ( $L = 100 \mu\text{m}$ ; $N_{max} = 4$ )	$100 < D_{max} < 1000 \mu\text{m}$	1.39	1.26
	rosettes ( $L = \sqrt{H}$ ; $N_{max} = 4$ )	$100 < D_{max} < 1000 \mu\text{m}$	1.65	2.16
	rosettes ( $L = 0.5H$ ; $N_{max} = 5$ )	$500 < D_{max} < 2000 \mu\text{m}$	1.83	2.9
	rosettes ( $L = 0.25H$ ; $N_{max} = 6$ )	$500 < D_{max} < 2500 \mu\text{m}$	1.78	2.97
	rosettes ( $L = 100 \mu\text{m}$ ; $N_{max} = 6$ )	$100 < D_{max} < 1000 \mu\text{m}$	1.42	1.25
	rosettes ( $L = \sqrt{H}$ ; $N_{max} = 6$ )	$100 < D_{max} < 1000 \mu\text{m}$	1.66	2.16
	capped columns (2 plates: $L_2 = 2.5L_1$ ; $H = L_1$ )	$150 < D_{max} < 1400 \mu\text{m}$	1.79	2.21
	capped columns (2 thick stars: $L_2 = 2.5L_1$ ; $H = L_1$ )	$150 < D_{max} < 1400 \mu\text{m}$	1.92	2.43
	$8 < N_{agg} < 30$ thick stars ( $H = \sqrt{L}$ ) individual diameter of thick stars : $30 < L < 40 \mu\text{m}$	$1000 < D_{max} < 4000$	1.79	1.92
	$8 < N_{agg} < 30$ plates ( $H = 0.1 * L$ ) individual diameter of plates : $20 < L < 30 \mu\text{m}$	$600 < D_{max} < 2000$	1.8	1.81
	$8 < N_{agg} < 30$ plates ( $H = \sqrt{L}$ ) individual diameter of plates : $20 < L < 30 \mu\text{m}$	$600 < D_{max} < 2500$	1.59	1.69
	$2 < N_{agg} < 4$ ; columns ( $L = 160 \mu\text{m}$ ) individual diameter of columns : $40 < H < 60$	$400 < D_{max} < 1500$	1.26	1.75
	$2 < N_{agg} < 4$ ; columns ( $L = \sqrt{H}$ ) individual diameter of columns : $40 < H < 60$	$200 < D_{max} < 1000$	1.45	2.07
	$2 < N_{agg} < 4$ ; thick stars ( $H = 0.2 * L$ ) individual diameter of thick stars : $40 < L < 60 \mu\text{m}$	$400 < D_{max} < 3000$	1.82	2.62
	$2 < N_{agg} < 4$ ; thick stars ( $H = 0.1 * L$ ) individual diameter of thick stars : $40 < L < 60 \mu\text{m}$	$400 < D_{max} < 3000$	1.63	2.62
	$2 < N_{agg} < 4$ ; thick stars ( $H = 40 \mu\text{m}$ ) individual diameter of thick stars : $40 < L < 60 \mu\text{m}$	$400 < D_{max} < 3000$	1.87	2.25
	$2 < N_{agg} < 4$ ; thick stars ( $H = \sqrt{L}$ ) individual diameter of thick stars : $40 < L < 60 \mu\text{m}$	$400 < D_{max} < 3000$	1.72	2.46
	$2 < N_{agg} < 4$ ; thin stars ( $H = 0.2 * L$ ) individual diameter of thin stars : $30 < L < 60 \mu\text{m}$	$300 < D_{max} < 2000$	1.64	2.52
	$2 < N_{agg} < 4$ ; thin stars ( $H = 0.1 * L$ ) individual diameter of thin stars : $30 < L < 50 \mu\text{m}$	$300 < D_{max} < 1500$	1.72	2.52
	$2 < N_{agg} < 4$ ; thin stars ( $H = 40 \mu\text{m}$ ) individual diameter of thin stars : $30 < L < 50 \mu\text{m}$	$300 < D_{max} < 1500$	1.46	2.14
	$2 < N_{agg} < 4$ ; thin stars ( $H = \sqrt{L}$ ) individual diameter of thin stars : $30 < L < 50 \mu\text{m}$	$300 < D_{max} < 2000$	1.53	2.37
	$2 < N_{agg} < 4$ ; plates ( $H = 0.2 * L$ ) individual diameter of plates : $30 < L < 50 \mu\text{m}$	$300 < D_{max} < 2000$	1.87	2.57
	$2 < N_{agg} < 4$ ; plates ( $H = 0.1 * L$ ) individual diameter of plates : $30 < L < 50 \mu\text{m}$	$250 < D_{max} < 1500$	1.61	2.37
	$2 < N_{agg} < 4$ ; plates ( $H = 40 \mu\text{m}$ ) individual diameter of plates : $30 < L < 50 \mu\text{m}$	$250 < D_{max} < 1500$	1.64	1.99
	$2 < N_{agg} < 4$ ; plates ( $H = \sqrt{L}$ ) individual diameter of plates : $30 < L < 60 \mu\text{m}$	$250 < D_{max} < 1500$	1.76	2.29
	$3 < N_{agg} < 20$ ; spheres individual diameter of spheres : $D = 60 \mu\text{m}$ ;	$300 < D_{max} < 2000 \mu\text{m}$	1.45	1.74
	$3 < N_{agg} < 50$ ; spheres individual diameter of spheres : $D = 150 \mu\text{m}$ ;	$100 < D_{max} < 1000 \mu\text{m}$	1.54	1.84

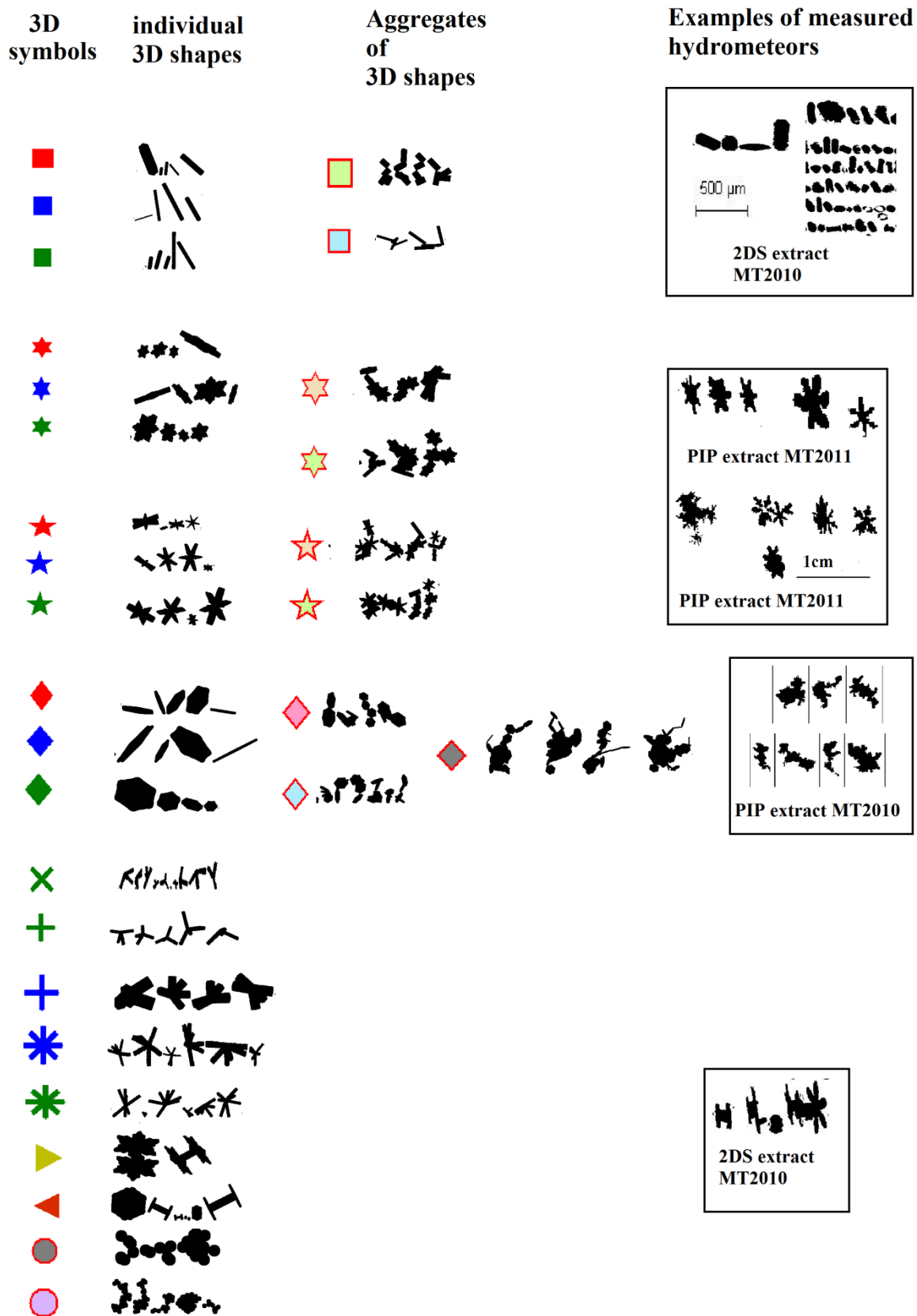


Figure 18 : On the left column are presented examples of 2D projections of randomly oriented 3D shapes of single hydrometeors with their corresponding symbols as they are represented in figure 7 and in table 4. In the middle column, examples of aggregates composed of single individual shapes as shown in the left column. The right column shows examples of crystals resembling what has been recorded in different aircraft measurement campaigns.

For each random orientation, it is possible to calculate a density. How do those density values compare to those determined by your mass dimensional relationships?

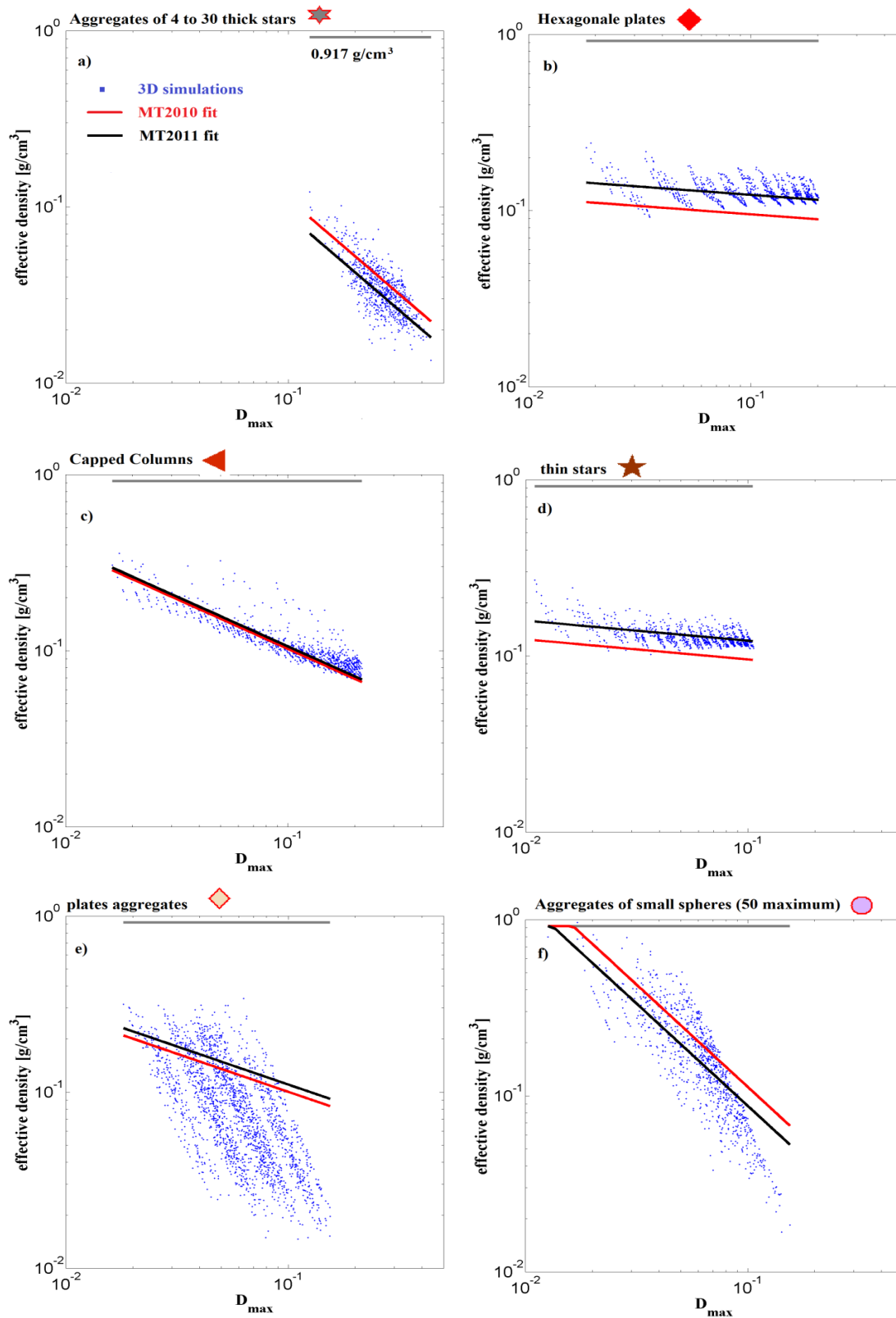


Figure 19 : Blue dots show effective density calculated from 3D simulations, which are compared with linear fits of  $\ln(\alpha)$  as a function of  $\beta$ , found for MT2010 (red line) and MT2011 (black line).

4. Using the alpha and beta values given in the summary for the mass dimensional relationship, I get  $m=0.0244 \cdot D^{2.44}$  or  $m=0.0266 \cdot D^{2.44}$ . This is really heavy for large particles, and substantially different for published mass dimensional relationships. The authors need to explain why there is such a substantial difference. Is it specifically related to your dataset? Or, are all of the others wrong, and if so, why?

*Mass-diameter relationships are calculated in this study with the help of measured reflectivity at 94GHz. Subsequently CWC can be calculated from PSD and  $m(D)$ . Most recently the international HAIC-HIWC campaign which took place during January- March 2014 out of Darwin allowed to confront the radar reflectivities of the RASTA radar and the direct measurements of the IWC using the IKP (isokinetic evaporator probe). This confrontation allowed to improve the method correcting the radar reflectivity close to the aircraft within 900m below and above the aircraft.*

*We integrated into our answers to the reviewers and in the new version of the radar RASTA data these results taking into account the corrections of the reflectivity of RASTA in the vicinity of the aircraft.*

*With the corrected new dataset of radar reflectivities we have then recalculated the mean  $m$ - $D$  coefficients. For example if the 2DS is solely used to calculate  $\sigma$  of the  $S$ - $D$  power law, and then calculate the  $m$ - $D$  exponent  $\beta$  and constrain  $\square$ , we find for:*

$$MT2010 : m(D_{\max}) = 0.0098 \cdot D_{\max}^{2.26}$$

$$MT2011 : m(D_{\max}) = 0.0082 \cdot D_{\max}^{2.22}$$

*And when  $\sigma$  is calculated from the 2DS plus the PIP images we receive :*

$$MT2010 : m(D_{\max}) = 0.0093 \cdot D_{\max}^{2.25}$$

$$MT2011 : m(D_{\max}) = 0.0057 \cdot D_{\max}^{2.06}$$

*These mean values of  $m$ - $D$  relationships are presented in the revised manuscript and are compared with other  $m$ - $D$  relationships in the new manuscript.*

Further comments:

Page 2984 line 2: Ice hydrometeors (without the word “ice” you could be talking about rain as well).

*“In this study the density of ice hydrometeors in tropical clouds is derived from a combined analysis of particle images of 2-D array probes...”*

Page 2987 lines 9-12: Relationships derived in SH2010 were derived numerically, and tested with aircraft data. (See major point #1 above).

Page 2987 line 13: There should be a period at the end of this line.

*“Schmitt and Heymsfield (2010, hereafter SH2010) have simulated the aggregation of plates and columns. Fractal 2D and 3D analyses calculated from the box counting method (Tang and Marangoni 2006) stated that the fractal coefficient in the 3D space is equal to  $\beta$ . This allowed to derive a relationship that calculates the exponent  $\beta$  from the 2D fractal dimension of the 2D images. Once  $\beta$  has been fixed, the pre-factor  $\alpha$  is calculated from the area measurement.”*

*Heymsfield et al. (2010, hereafter H10) demonstrate that a strong relationship exists between  $\alpha$  and  $\beta$  coefficients and argue that the BF95 relationship overestimates the prefactor  $a$  for stratiform clouds, whereas  $a$  is underestimated for convective clouds. “*

Page 2988 line 21: Was the Nevzorov probe used a standard version or modified with a deeper groove? The standard version likely underestimates CWC when there are high concentrations of larger particles which can shatter and partially bounce out on impact. (See Korolev's 2011 BAMS article)

*Yes we use the deep cone version of the Nevzorov.*

Page 2990 line 8: TSD is not defined. Could you mean AsD?

*“Examples of PSD and AsD are presented in Fig. 1...”*

Page 2990 line 24: How do the measured aspect ratio values from the probe measurements compare to the average aspect ratio calculated for the theoretical particles (in the appendix)? (Densities as well)

*Average aspect ratio of theoretical simulations may not be entirely comparable with experimentally measured average As due to possible orientation of crystals. In case that crystals are sampled randomly oriented on the aircraft, simulations and observations of As are fully comparable.*

Page 2991 line 24: You assume that the reflectivity at the aircraft is the value linearly interpolated between the value 300m above and the value 300m below. How different are these values typically? Difference and standard deviation and how much uncertainty does this cause in the results? It might be interesting to look at the difference between 300 and 900 meters above and see if that difference is similar to the difference between 300 above and 300 below.

*Reflectivity differences between the Nadir antenna and Zenith antenna 300 m above and 300 m below the aircraft are of the same order than the differences between 300 and 900 meters above and also below. These differences are in the range of about [1.6 - 3.5dBZ], with an exception for the flight 49 of MT2011. Clouds in this flight were very small isolated convective flight and were not taking into account to calculate the mean mass-diameters coefficients.*

*A linear interpolation of measured reflectivities below and/or beyond the aircraft in order to estimate the reflectivity at the aircraft flight altitude, would result in a maximum uncertainty of the estimated reflectivity at flight level of 2dBZ, which means a maximum error of 20% on the retrieved CWC.*

Table 4: Mean difference in dBZ and standard deviation of RASTA reflectivities calculated between two radar gates having a distance of 600 meters.

Flight	$Z_{Zenith(300m)} - Z_{Zenith(900m)}$		$Z_{Nadir(300m)} - Z_{Nadir(900m)}$		$Z_{Nadir(300m)} - Z_{Zenith(300m)}$	
	Mean [dBZ]	Std [dBZ]	Mean [dBZ]	Std [dBZ]	Mean [dBZ]	Std [dBZ]
15	3.16	2.82	3.45	4.03	3.22	3.33
17	2.94	2.81	3.00	3.06	2.56	2.59
18	2.07	2.43	2.49	2.75	1.59	2.13
19	4.33	3.82	2.98	3.51	3.46	3.52
20	2.68	2.50	2.66	2.55	1.6	1.68
45	4.24	4.01	3.69	3.93	3.33	3.28
46	4.98	4.39	3.76	3.94	3.36	3.58
49	6.43	5.41	7.34	6.77	5.11	5.69
50	4.56	6.11	4.81	6.49	2.10	5.69

Page 2992 & figure 4: Doesn't 5 g/m3 CWC seem rather high? Your dBZ values are very high. My concern is that the Protat 2007 parameterization appears to include data only up to about 10dBZ. Could higher values be influenced by graupel or hail? This should show up in the PIP data.

*We do not understand why you refer the  $5\text{g}/\text{m}^3$  to the Protat 2007 parametrisation, knowing that the Protat parameterization was not used to calculate the retrieved CWC used in this study.*

*However, as we can see in figure 6, during the high IWC ( $5\text{g}/\text{m}^3$ ), 2D images recorded by the PIP show few graupels with a size around 1mm to 2mm.*

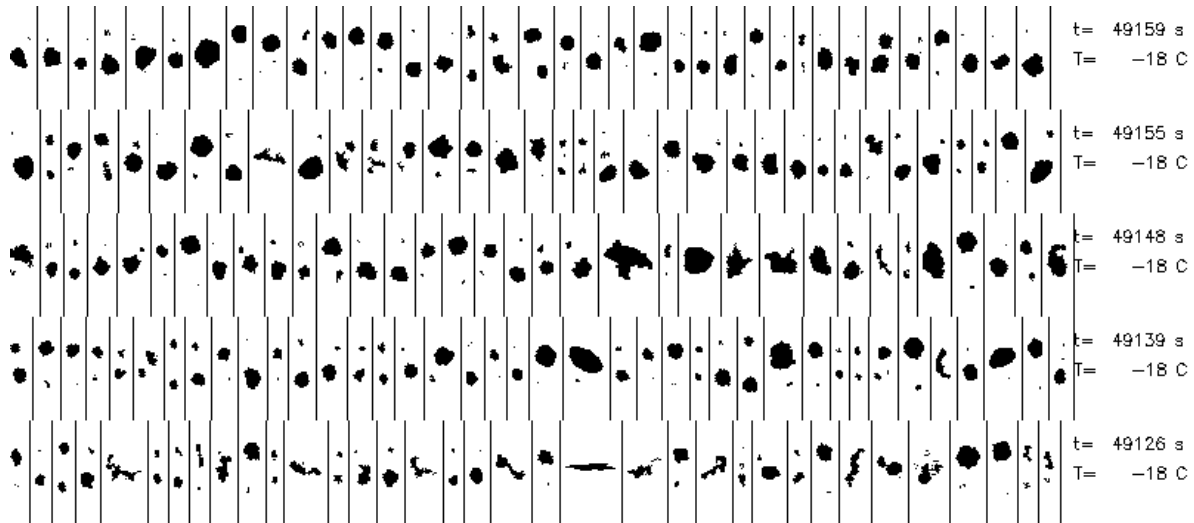


**Figure 20: Extract of PIP image catalogue of flight 18. Bars between 2 particles constitute 7mm in length.**

Figure 4 should also have the dBZ value derived for the pass.

*We do not understand the question.*

Page 2994 line 13: Suggest that you try the Schmitt and Heymsfield method for calculating alpha directly from the particle area data and compare to your results.

*Implementing the Schmitt and Heymsfield method is beyond the scope of this study. We are not sure of having all the details to implement and run the method.*

Page 2995: Sigma for each particle shape is calculated, but it is unclear how.

*The  $\sigma$  is calculated for the entire population of crystals imaged during 5 seconds with 2D-S plus PIP probes. The method is explained above in answering to your comment 2 in the beginning.*

Is the area and maximum dimension determined for each random orientation, then a fit done to maximum dimension versus area for all of the individual rotations? If so, then your sigma value may be more related to the orientation rather than the size to area relationship.

*Each 3D crystal shape includes 1000 simulations where the crystal size and orientation varied in the 3D space. There is only one power fit for  $m(D_{max})$  and  $S(D_{max})$  per single 3D crystal shape (including size and orientation variation) (see also answer to the comment 2 and figure 1 and Appendix A on the current version of the paper).*

*Of course the  $m(D_{max})$  and  $S(D_{max})$  are related to the 3D orientation, however, also  $D_{max}$  is dependent on the 3D orientation.*

Page 2995 line 21-22: using 1.0 for sigma yields a value of 0.6 for beta (outside the range presented on line 21).

*Taken into account the added simulations and orientations uncertainties now we have:  
 $\beta = 1.93 \cdot \sigma - 1.02$  (equation 11 in the current version), with  $\sigma$  in the range [1.05 ; 2].*

Page 2995: How many of your theoretical particles are truly irregular? How many of your observed particles are truly irregular?

*See new version of figure 6 in the answer to the comment 3.*

Page 2997, line 17: Consider comparing either Brown and Francis and/or Heymsfield et al 2004. There are no assumptions on shapes in these as well.

*An extended study on the impact of the variability of  $m(D)$  coefficients on CWC and CWC-Z, including Brown & Francis has been added in the revised version of the manuscript; see also answer to the second reviewer for all the details.*

Page 2998 line 25: From here, there is a lot of discussion of the basic properties of the clouds measured during the campaigns. It isn't clear why it is important to discuss this now. Much of it isn't relevant to the study.

*This part has been removed in order to take into account, the comments of referee #2 and #3.*

Page 3001 line 3: It would be interesting to plot some typical density values from your alpha beta pairs as compared to density values from the literature.

*Averaged values of  $m(D)$  coefficients found for MT2010 and MT2011 with  $\alpha$  determined from 2DS only are relatively close. They give less mass for a same  $D_{max}$  if they are compared with  $m(D)$  coefficients of H2010 for NAMMA. Average values for  $m(D)$  coefficients when 2DS plus PIP are used to determine  $\alpha$ , show similar trends between H2010 for cloud convectively generated and MT2011.  $m(D)$  coefficients given by Mitchell 1996 give less mass for a same  $D_{max}$  compared with the  $m(D)$  relationships cited before, with an exception for the lump graupel's  $m(D)$  coefficients which give largest mass for particles beyond 1mm compared to all the other  $m(D)$  relationships. Mitchell's lump graupel still give larger mass for particles beyond 500 $\mu$ m compared to MT2010 and MT2010  $m(D)$  from T-matrix and H2010 convectively generated  $m(D)$ .*

*Note that for MT2010 when using the 2DS plus PIP to determine  $\alpha$  we find  $m(D)$  coefficients close to those found with 2DS with  $\alpha=0.0093$  and  $\beta=2.25$*

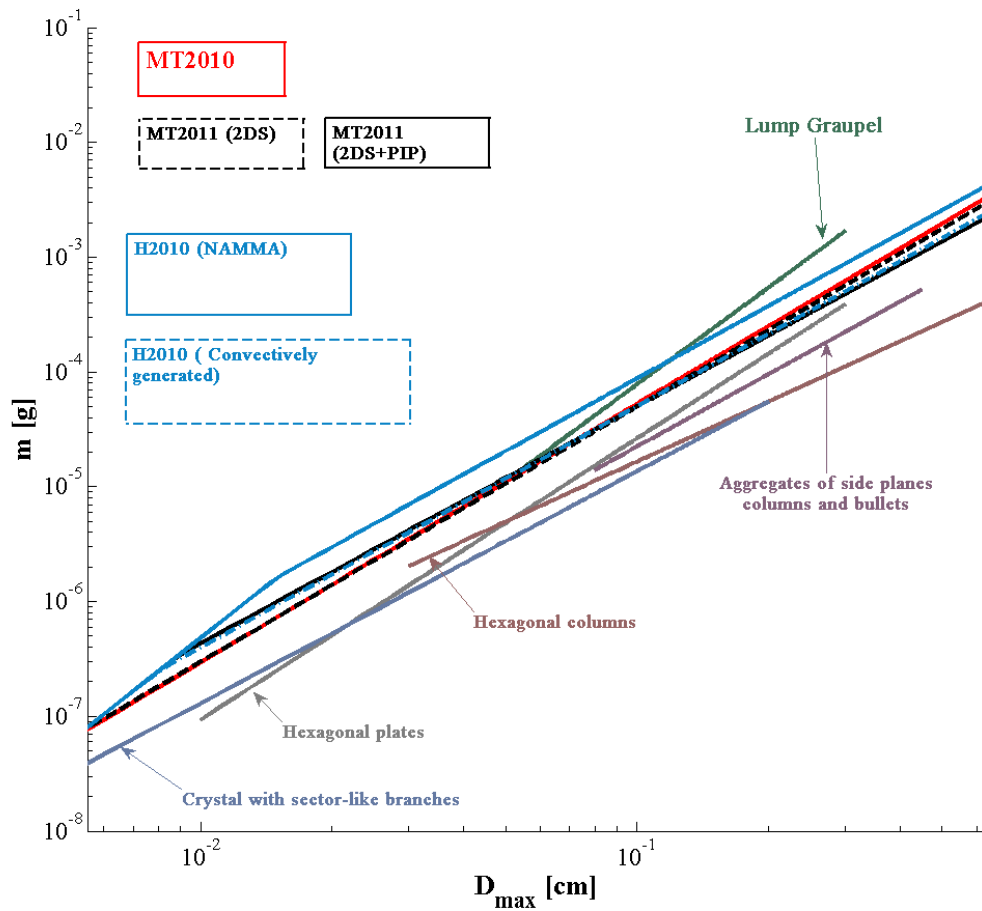


Figure 21 : Mass of ice crystals in gram on y axis, as a function of their  $D_{max}$  in cm on the x axis. The red line represents mean values of  $m(D)$  coefficients for MT2010 when  $\sigma$  is determined from 2D-S plus PIP images with  $\alpha=0.0098$  and  $\beta=2.26$ . Likewise, the black dashed line represents  $m(D)$  coefficients for MT2011 with  $\alpha=0.0057$  and  $\beta=2.06$ . The black line represents MT2011 when  $\sigma$  is determined from 2DS only with  $\alpha=0.0082$  and  $\beta=2.22$ . The blue line represents  $m(D)$  coefficients taken from H2010 for the NAMMA campaign with  $\alpha=0.011$  and  $\beta=2.1$ . Dashed blue line stands for H2010, but for convectively generated systems with  $\alpha=0.0063$  and  $\beta=2.1$ . Blue grey line is given by Mitchell 1996 for crystal with sector-like branches with  $\alpha=0.00142$  and  $\beta=2.02$ . Grey line (Mitchell 1996) represents hexagonal plates with  $\alpha=0.00739$  and  $\beta=2.45$ . Brown grey line (Mitchell 1996) represents hexagonal columns with  $\alpha=0.000907$  and  $\beta=1.74$ . Purple grey line (Mitchell 1996) is for aggregates of side planes columns and bullets with  $\alpha=0.0028$  and  $\beta=2.1$ . Green line (Mitchell 1996) is for Lump Graupel with  $\alpha=0.049$  and  $\beta=2.8$ .

Given the extremely high dBZ values recorded, can these results be generalized?

*Results presented in this study have been compared to other methods of  $m(D)$  estimations. Details are given in the answer to reviewer nr.2 and in the revised version of the manuscript. The variability of  $m(D)$  coefficients from T-matrix retrievals as a function of the temperature is similar to the one presented by SH2010 (more details in answer to comments of Referee 1*

and 2),

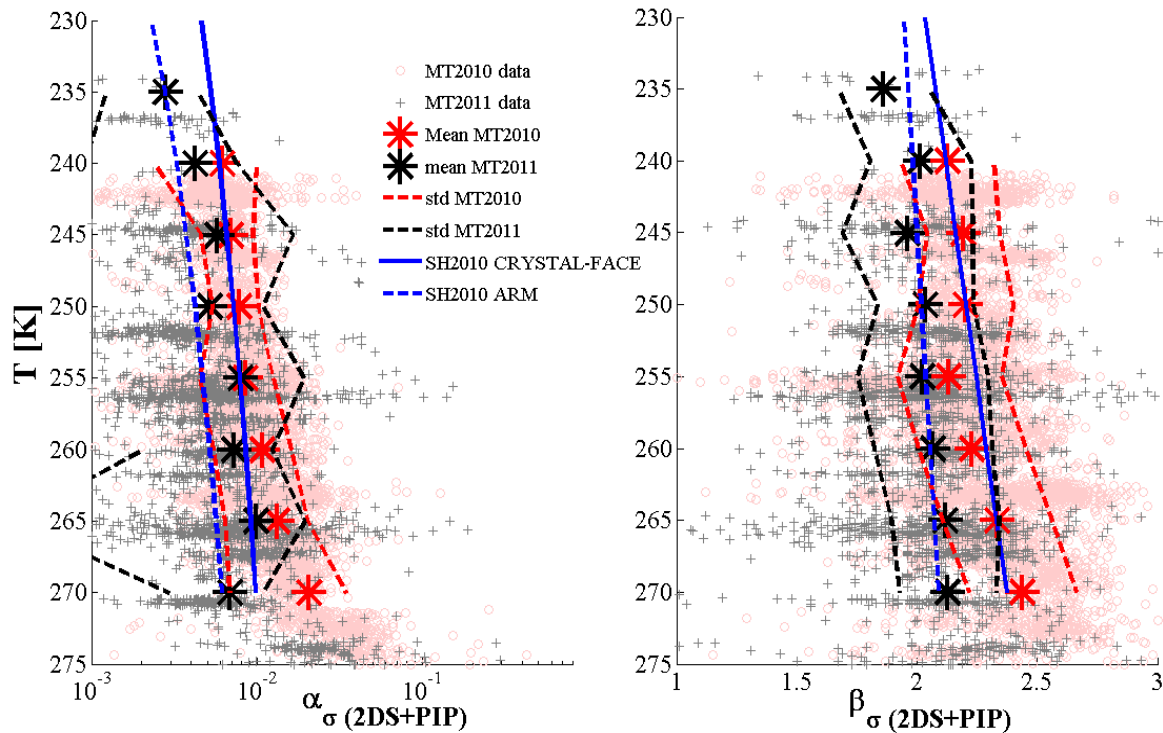


Figure 22 : Vertical profile of  $m(D)$  coefficients constrained by T-matrix and the variability of S-D exponent  $\square$  calculated from 2D-S plus PIP images. (a)  $\alpha_{\sigma}$  versus the temperature in K. (b)  $\beta_{\sigma}$  versus the temperature in K. Pink circle show data points (5-seconds time step) of MT2010, grey crosses show MT2011 data. Red and black stars present mean values of  $m(D)$  coefficients in 5K temperature intervals for MT2010 and MT2011, respectively. Dashed red and black lines show standard deviations of MT2010 and MT2011, respectively, from the mean value. Blue solid and dashed lines show vertical profiles of SH2010 obtained for CRYSTAL-FACE, and for ARM, respectively.

Page 3004 line 4-5: When I compare these alpha and beta pairs to BF, the results show a similar density predicted for 200 micron particles, then for larger (3000 um) up to a factor of 5 higher density for your results. This difference (with BF and others) needs to be shown and explained.

*Brown and Francis relationships were calculated for  $D=(L_x+L_y)/2$ , where  $L_y$  is the size along the array diode and  $L_x$  the size perpendicular to  $L_y$ , whereas  $D_{max}$  is the size of the circle which englobes the entire 2D image. Therefore, due to discrepancies in diameter definition, BF seems not appropriate to be compared on a same plot with mass versus  $D_{max}$ .*

Page 3006 line 9: It would be good to show typical plots of the shape of the PSDs so that they can be compared to other data. Gamma fit parameters ( $\lambda$ ,  $\mu$ ,  $N_0$ ) as are commonly shown would be helpful.

*PSD cannot be easily fitted with Gamma distributions, the concentration of small ice hydrometeors would be badly represented. Start fitting the PSD would end in adding a somewhat different topic to that manuscript. The idea should be followed up, preparing a separate study on fitting of PSD for available data sets.*

## List of relevant changes made in the manuscript

A new co-author is added. C. Goubeyre<sup>1</sup>

Sections 3, 4, 5 and 6 are change in order to advance the variability of mass-diameter relationships.

New summary :

Constraining Mass-Diameter Relations from Hydrometeor Images and Cloud Radar Reflectivities in Tropical Continental and Oceanic Convective Anvils

E. Fontaine<sup>1</sup>, A. Schwarzenboeck<sup>1</sup>, J. Delanoë<sup>2</sup>, W. Wobrock<sup>1</sup>, D. Leroy<sup>1</sup>, R. Dupuy<sup>1</sup>, C. Goubeyre<sup>1</sup>, A. Protat<sup>2,\*</sup>

Abstract.....	1
1 Introduction .....	2
2 Cloud data from the Megha-Tropiques flight campaigns .....	5
3 Methodology of m(D) retrieval: Studying 2D and 3D aspects of hydrometeors .....	8
3.1 Simulations of artificial ice crystal shapes and associated S(D) and m(D).....	8
3.2 Surface-diameter relationships of natural hydrometeors .....	10
3.3 Mass-diameter coefficients and CWC retrieval .....	11
3.4 Impact of measurement uncertainties on m(D) and CWC retrieval .....	15
4 m(D) relationship and impact on Z-CWC calculation.....	16
4.1 m(D) variability.....	16
4.2 m(D) impact on Z-CWC and Z-CWC-T.....	19
5 Discussion and Conclusion .....	21
APPENDIX A: Description of 3D simulations .....	23
Plates.....	24
Columns .....	24
Slender Stellars and more solid stellars .....	24
Capped Columns .....	24
Rosettes.....	25

Aggregates of individual crystal shapes .....	25
APPENDIX B: List of Symbols .....	26
Acknowledgments.....	28
References .....	28

Tables changes:

Tables 4 (in the old version) becomes Tables 2 (in the revised version), it includes new results from 3D simulations of crystals aggregates.

Tables 2 (in the old version) becomes Tables 3 (in the revised version).

Tables 3 (in the old version) becomes Tables 4 (in the revised version).

Table 5 in the old version is removed.

In the revised version of the paper, Table 5, Table 6, Table 7 and Table 8 are added.

Figures changes:

Figure 16 (in the old version) becomes Figure 1 (in the revised version).

Figure 1 (in the old version) becomes Figure 2 (in the revised version).

Figure 6 (in the old version) becomes Figure 3 (in the revised version). Images of simulated crystals are stored by habits with examples of similar real ice crystals.

Figure 7 (in the old version) becomes Figure 4 (in revised version). Symbols of simulated crystals aggregates are added, as the uncertainty of the fitted linear relationships between  $\sigma$  and  $\beta$ .

Figure 5 is added (in the revised version) to show examples of Surface-diameter relationships from the Megha-Tropiques dataset.

Figure 2 (in the old version) becomes Figure 6 (in the revised version).

Figure 3 (in the old version) becomes Figure 7 (in the revised version).

Figure 4 in the old version is deleted.

In figure 8 the  $CWC(\alpha_i, \beta_i)$  is removed.

Figure 5 (in the old version) becomes Figure 9 (in the revised version).

Figure 9 (in the old version) becomes Figure 10 (in the revised version), and Figure 9c is removed.

Figure 10 (in the old version) becomes Figure 11 (in the revised version).

Figure 12 in the new version is added, showing a comparison of mass-diameter relationships from this study and present in the literature.

Figure 11b) et 11c) (in the old version) becomes Figure 13a) and 13b) (in the revised version). Others parts of the Figure 11 are deleted.

Figure 12, and 13 in the old version are deleted.

Figure 14 (in the old version) becomes Figure 14a) and 14b) (in the revised version).

Figure 15 is added in the revised version, in order to show Z-CWC-T relationships.

Figure 15 (in the old version) becomes Figure 16a) (in the revised version). Probability Distribution function of mean aspect ratio of MT2010 and MT2011 are added in Figure 16b) and 16c).

In the appendix, Figure A1 is added in the revised version.

Figure A1 (in the old version) becomes Figure A2 (in the revised version).

Figure A2 (in the old version) becomes Figure A3 (in the revised version).

Figure A3 (in the old version) becomes Figure A4 (in the revised version).

Figure A4 (in the old version) becomes Figure A7 (in the revised version).

#### New references are added :

Bailey, M., and J. Hallett, 2004: Growth Rates and Habits of Ice Crystals between  $-20^{\circ}$  and  $-70^{\circ}\text{C}$ . *J. Atmospheric Sci.*, **61**, 514–544, doi:10.1175/1520-0469(2004)061<0514:GRAHOI>2.0.CO;2.

Bailey, M. P., and J. Hallett, 2009: A Comprehensive Habit Diagram for Atmospheric Ice Crystals: Confirmation from the Laboratory, AIRS II, and Other Field Studies. *J. Atmospheric Sci.*, **66**, 2888–2899, doi:10.1175/2009JAS2883.1.

Cetrone, J., and R. A. Houze, 2009: Anvil clouds of tropical mesoscale convective systems in monsoon regions. *Q. J. R. Meteorol. Soc.*, **135**, 305–317, doi:10.1002/qj.389.

Frey, W., and Coauthors, 2011: In situ measurements of tropical cloud properties in the West African Monsoon: upper tropospheric ice clouds, Mesoscale Convective System outflow, and subvisual cirrus. *Atmospheric Chem. Phys.*, **11**, 5569–5590, doi:10.5194/acp-11-5569-2011.

Heymsfield, G. M., L. Tian, A. J. Heymsfield, L. Li, and S. Guimond, 2010b: Characteristics of Deep Tropical and Subtropical Convection from Nadir-Viewing High-Altitude Airborne Doppler Radar. *J. Atmospheric Sci.*, **67**, 285–308, doi:10.1175/2009JAS3132.1.

Hogan, R. J., L. Tian, P. R. A. Brown, C. D. Westbrook, A. J. Heymsfield, and J. D. Eastment, 2011: Radar Scattering from Ice Aggregates Using the Horizontally Aligned Oblate

Spheroid Approximation. *J. Appl. Meteorol. Climatol.*, **51**, 655–671, doi:10.1175/JAMC-D-11-074.1.

Houze, R. A., 2004: Mesoscale convective systems. *Rev. Geophys.*, **42**, n/a–n/a, doi:10.1029/2004RG000150.

Jensen, E., D. Starr, and O. B. Toon, 2004: Mission investigates tropical cirrus clouds. *Eos Trans. Am. Geophys. Union*, **85**, 45–50, doi:10.1029/2004EO050002.

Jensen, M. P., and A. D. Del Genio, 2003: Radiative and Microphysical Characteristics of Deep Convective Systems in the Tropical Western Pacific. *J. Appl. Meteorol.*, **42**, 1234–1254, doi:10.1175/1520-0450(2003)042<1234:RAMCOD>2.0.CO;2.

Kobayashi, R., 1993: Modeling and numerical simulations of dendritic crystal growth. *Phys. Nonlinear Phenom.*, **63**, 410–423, doi:10.1016/0167-2789(93)90120-P.

Liu, C.-L., and A. J. Illingworth, 2000: Toward More Accurate Retrievals of Ice Water Content from Radar Measurements of Clouds. *J. Appl. Meteorol.*, **39**, 1130–1146, doi:10.1175/1520-0450(2000)039<1130:TMAROI>2.0.CO;2.

Maxwell Garnet, J. C., 1904: Colours in Metal Glasses and in Metallic Films. *Philos. Trans. R. Soc.*, 385–420, doi:10.1098/rsta.1904.0024.

Tang, D., and A. G. Marangoni, 2006: 3D fractal dimension of fat crystal networks. *Chem. Phys. Lett.*, **433**, 248 – 252, doi:http://dx.doi.org/10.1016/j.cplett.2006.11.057.

Toon, O. B., D.O. Starr, E.J. Jensen, P.A. Newman, S. Platnick, M.R. Schoeberl, P.O. Wennberg, S.C. Wofsy, M.J. Kurylo, H. Maring, K.W. Jucks, M.S. Craig, M.F. Vasques, L. Pfister, K.H. Rosenlof, H.B. Selkirk, P.R. Colarco, S.R. Kawa, G.G. Mace, P. Minnis and K.E. Pickering, 2010: Planning, implementation, and first results of the Tropical Composition, Cloud and Climate Coupling Experiment (TC4). *J. Geophys. Res. Atmospheres*, **115**, n/a–n/a, doi:10.1029/2009JD013073.

Westbrook, C. D., R. C. Ball, P. R. Field, and A. J. Heymsfield, 2004: Theory of growth by differential sedimentation, with application to snowflake formation. *Phys Rev E*, **70**, 021403, doi:10.1103/PhysRevE.70.021403.

Zikmunda, J., and G. Vali, 1972: Fall Patterns and Fall Velocities of Rimed Ice Crystals. *J. Atmospheric Sci.*, **29**, 1334–1347, doi:10.1175/1520-0469(1972)029<1334:FPAFVO>2.0.CO;2.

Zipser, E. J., C.H. Twohy, S-C. Tsay, N.C. Hsu, G.M. Heymsfield, K.L. Thornhill, S. Taneli, R. Robert, T.N. Krishnamurti, Q. Ji, G. Jenkins, S. Ismail, R. Ferrare, G. Chen, E.V. Browell, B. Anderson, R. Hood, H.M. Goodman, A.J. Heymsfield, J. Halverson, J.P. Dunion, M. Douglas and R. Cifelli, 2009: The Saharan Air Layer and the Fate of African Easterly Waves—NASA’s AMMA Field Study of Tropical Cyclogenesis. *Bull. Am. Meteorol. Soc.*, **90**, 1137–1156, doi:10.1175/2009BAMS2728.1.